ACS OMEGA

Open Access

http://pubs.acs.org/journal/acsodf

Review

La-Fe-O Perovskite Based Gas Sensors: Recent Advances and Future Challenges

Suraj S. Patil, Bapuso M. Babar, Digambar Y. Nadargi,* Faiyyaj I. Shaikh, Jyoti D. Nadargi, Babasaheb R. Sankapal, Imtiaz S. Mulla, Mohaseen S. Tamboli, Nguyen Tam Nguyen Truong,* and Sharad S. Suryavanshi*

Cite This: *ACS Omega* 2024, 9, 29994−30014

Read Online

ACCESS | Metrics & More | Article Recommendations

ABSTRACT: Interest in the importance of gas sensing devices has increased significantly due to their critical function in monitoring the environment and controlling pollution, resulting in an increased market demand. The present review explores perovskite La-Fe-O based gas sensors with a special focus on $LaFeO_3$ and evaluates their sensitivity to a diverse range of practical target gases that need to be monitored. An analysis has been conducted to assess different routes not only of synthesizing $LaFeO_3$ material but also of characterization with the targeted use for their gas sensing abilities. Additionally, a comprehensive analysis has been performed to explore the effect of introducing other elements through doping. In view of the $LaFeO_3$ sensing performance, more common gases like acetone, ethanol, methanol, formaldehyde, NO_x, and CO_2 have been targeted. In addition, a discussion on uncommon gases such as CO, SO_2, TEA, C_2H_5, C_6H_6, and others is also made to give a complete picture of $LaFeO_3$-based gas sensors. The summary and conclusion section of the study addresses the primary obstacles in the synthesis process, the variables that restrict the sensing capabilities of $LaFeO_3$, and its commercial fulfillment.

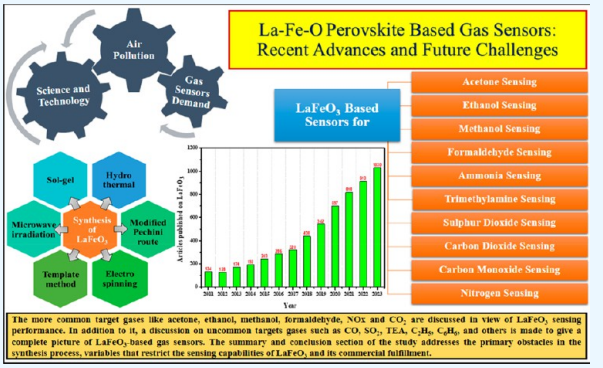

1. INTRODUCTION

The revolution in the field of science and technology has made human life easier. Particularly, advancement in the agricultural and industrial sectors has helped the economy boom, which is very essential for every nation's growth. However, on the other side of the coin, the adverse consequences of technological growth have been observed, which is of permanent importance to look into. Various hazardous gases and vapors are being released into the atmosphere, thereby generating air pollution. This issue has been designated as a primary concern in the majority of nations. Pollution in the air has a deleterious impact on all living things, including humans, animals, plants, and materials. Figure 1 illustrates the main reasons behind air pollution in developing countries. Basically, air pollution is primarily brought in due to presence of gases like NO_2, SO_2, CO, O_3, H_2S, and volatile organic compounds (VOCs) in the air.[1] Due to the fluidity and ability to spread, air pollution has a greater detrimental effect on human health systems.[2,3] As per research carried out worldwide in 2019, air pollution is a major part of pollution which contributes around 12% of fatalities. In addition, it has been claimed that air pollution was responsible for about 21% of the fatalities that were caused by cardiovascular illnesses.[4] Compared to adults, children are at greater risk of many adverse health effects of air pollution. Hence, not only chronic exposure but also acute exposure of pollutants of air is hazardous to human health.[5] As per research carried by environment protecting agencies, 92% of the world's population comes from cities which exceeded the level of pollutants in air according to WHO guidelines.[6−8] The study shows an urgent need for monitoring and controlling air pollution.

Consequently, it is of the utmost importance to work on developing highly sensitive sensors that can detect harmful gases at low ppm concentrations at room temperature (RT) or relatively low temperature. Moreover, these sensors need to be of high quality in terms of quick response/recovery, sensitivity, and stability toward a wide range of volatile gases/organic compounds. Therefore, there is a significant amount of scope for growth in the domain of gas sensors research and

Received: January 10, 2024
Revised: May 18, 2024
Accepted: May 29, 2024
Published: July 1, 2024

Figure 1. Illustration of causes and main resources responsible for the sudden growth in air pollution in urban areas of developing countries.

development. This review highlights aspects such as the need for gas sensors, its market study, and varieties of gas sensors available in the market. Particular attention is made to give an illustrative picture of chemiresistive perovskite-based gas sensors with a focus on lanthanum ferrite ($LaFeO_3$). Finally, a summary is given with a future scope in the field of perovskite-based gas sensors.

1.1. Market Study of the Gas Sensors. In recent years, several varieties of gas sensors including new wearable gas sensors for environmental and human health monitoring have been commercially accessible in the market.[9−13] The worldwide gas sensor market size was assessed at USD 823.1 million until 2019. Further, it is anticipated that it will reach USD 1,336.2 million by 2027, expanding at a compound annual growth rate (CAGR) of 6.4% from 2020 to 2027.[12] The significant factors that impact the growth of the global market for gas sensors include an increase in the use of gas sensors in the defense and military sectors, an emerging demand for gas sensors in consumer electronics, and favorable government regulation regarding the use of gas sensors. On the other hand, it is projected that the increasing trend toward the Internet of Things (IoT) and the rising use of sensors in the creation of smart cities would present profitable prospects for the gas sensors market in the near future. However, the high initial cost of the sensors serves as a key barrier for their adoption, which, in turn, impedes the development of the market.

On the working principles, the gas sensors available in the market are categorized as follows;

- **MEMS (Micro Electro Mechanical System) pellistors:** Mainly used to detect combustible gases. It works on the following principle: A sudden change in the temperature of the sensing material due to the oxidation of flammable gases which comes in contact with the sensor will result in the change in the resistance of the sensing material.
- **Catalytic pellistors:** In this pellistor, a thick film of catalyst is deposited onto the surface of an alumina bead, and a Pt wire is used to heat the catalyst. A sudden increase in the bead temperature indicates the presence of inflammable gas.
- **Thermal conductivity pellistors:** This sensor can only be used to detect the gases for which thermal conductivity is a significantly different value than the thermal conductivity of air. For example, hydrogen, helium, methane, etc. This device works by comparing the thermal conductivity of two different gases.
- **Infrared gas sensors:** In this sensor a beam of IR is used to detect the present gas and its concentration in the atmosphere.
- **Chemiresistive gas sensors:** The chemical reaction between the surface adsorbed oxygen and the gas molecules by forming electron depletion or a hole accumulation layer causes a change in the electrical resistance of the sensing element.
- **Electrochemical gas sensors:** In this type of sensor an electrochemical reaction causes a current in the external circuit.[14]

All of these gas detecting devices are primarily made up of two fundamental building elements, which are denoted by (a) receptors and (b) transducers. The receptor undergoes a change in its characteristics as a result of the target gas interaction, whereas transducers convert this change into appropriate signals. Figure 2 illustrates the list of available types of gas sensors in the market.

1.2. Chemiresistive Gas Sensors. The chemiresistive gas sensors have some appealing characteristics that differentiate them from other types of gas sensors which includes the need for a low heater current, a wide detection range, high sensitivity, portable devices, miniature dimensions, a long-life expectancy, suitability, high resistance to shocks, and vibrations

https://doi.org/10.1021/acsomega.4c00334
ACS Omega 2024, 9, 29994−30014

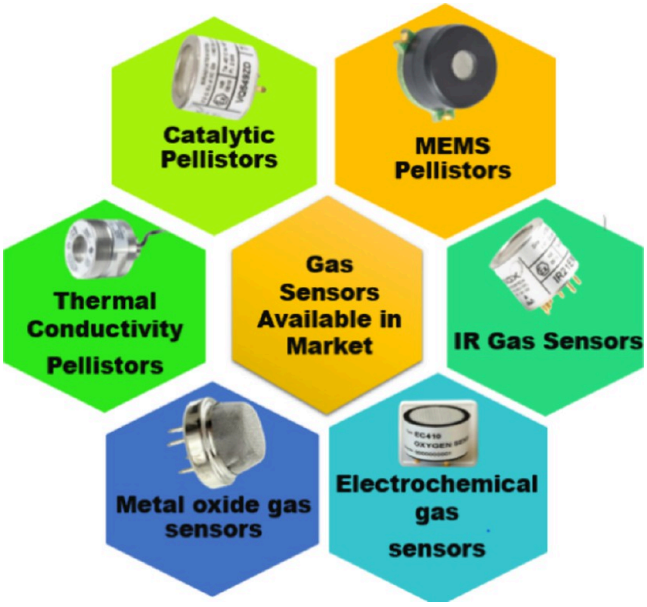

Figure 2. Gas sensors available in market (created by using images of products of AEP Components, Netherlands, https://www.aepint.nl/components).

for use in applications involving measurements or alarm warnings. The change in electrical resistance or conductance in the environment of target gas is the basic mechanism of gas sensing of a chemiresistive sensor. Initially in air, upon adsorption of oxygen molecules, an electron depletion layer (EDL) for n-type materials and a hole accumulation layer (HAL) for p-type materials will be formed on the sensor's surface.[1]

Particularly speaking, metal oxide semiconductor-based (MOS) sensors are capable of performing the functions of both receptors and transducers at the same time. At first, these semiconductors will create an electron depletion layer or a hole accumulation layer as a result of surface adsorption of oxygen in the air medium, thereby causing a change in the resistance (rise/fall), depending on the kind of the gas and the type of MOS. When a p-type metal oxide semiconductor is brought into contact with an oxidizing gas, the value of its resistance goes down, whereas the value of its resistance goes up when it comes into contact with a reducing gas. The statement is true in a reverse manner in the case of n-type semiconductors.[15]

1.3. Motivation of the Review Article. Figure 3a,b shows number of research articles over the period of the last ten years on gas sensors based on only common metal oxide semiconductors (MOS). It can be clearly seen that significantly less efforts and focus have been made for La-Fe-O based gas sensors as compared to other gas sensing materials like MnO_2, ZnO, WO_3, SnO_2, CuO, etc.[1,11−13,16−28] There is a wide range of research for other uncommon MoS, which is not attributed in the present graph.

Due to the easily tunable electronic properties by doping and the partial substitution of transition metals, $LaFeO_3$ has a good scope in the field of gas sensing applications.[29] Many researchers reported some versatile gas sensors based on $LaFeO_3$ and its compositions like $LaFeO_3/SnO_2$, $BaTiO_3/LaFeO_3$, $LaFeO_3/Fe_2O_3$, Ag-$LaFeO_3$, etc.[30−34] The motivation of the present review article is to give a detailed and systematic study of development in the field of $LaFeO_3$ based gas sensors which will offer key points for planning new strategies in the

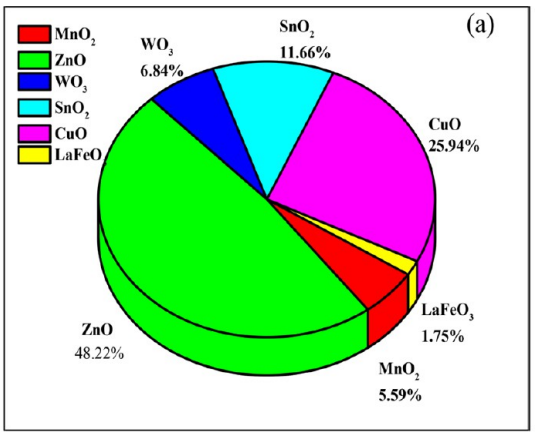

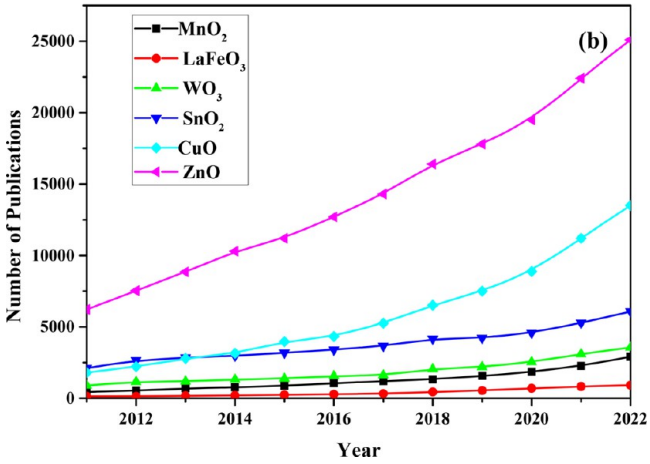

Figure 3. (a) Percentage of research articles published on MOS materials as gas sensors. (b) Number of research articles published in the field of gas sensing materials during the last ten years.

investigation of $LaFeO_3$ as a gas sensor. Figure 4 showcases the number of publications over the period of the last ten years in the field of $LaFeO_3$ gas sensors.

The initial identification of perovskites was accomplished by the Russian mineralogist Lev Perovski. The perovskite structure is predominantly observed in compounds with the general formula ABO_3, where A represents lanthanide or alkali earth metals, and B denotes a transition metal.[35] A few of the perovskite compositions are highlighted over here: $BiFeO_3$, $LaFeO_3$, $PrFeO_3$, $BaTiO_3$, $CaZrO_3$, $PbTiO_3$, and $CaSiO_3$. Figure 5 showcases the crystal structure of the ABX_3 perovskite.

These perovskites exhibit several notable characteristics, including a high absorption coefficient, low excitation binding energy, high dielectric constant, and enhanced charge transport capabilities. Extensive research has been conducted on transition metals incorporated in ABO_3 based perovskite structures, exploring their potential applications in various fields such as catalysis, fuel cell electrodes, colossal magneto-resistance, photocatalytic dye-degradation, supercapacitors, and gas sensing.[36−40]

$LaFeO_3$ exhibits superior gas sensing capabilities compared to other ABO_3 based perovskites due to its substantial surface area and abundance of surface-active sites. The strategic substitution of La and/or Fe atoms in $LaFeO_3$ allows for facile modification of its elemental composition. The substitution of

https://doi.org/10.1021/acsomega.4c00334
ACS Omega 2024, 9, 29994−30014

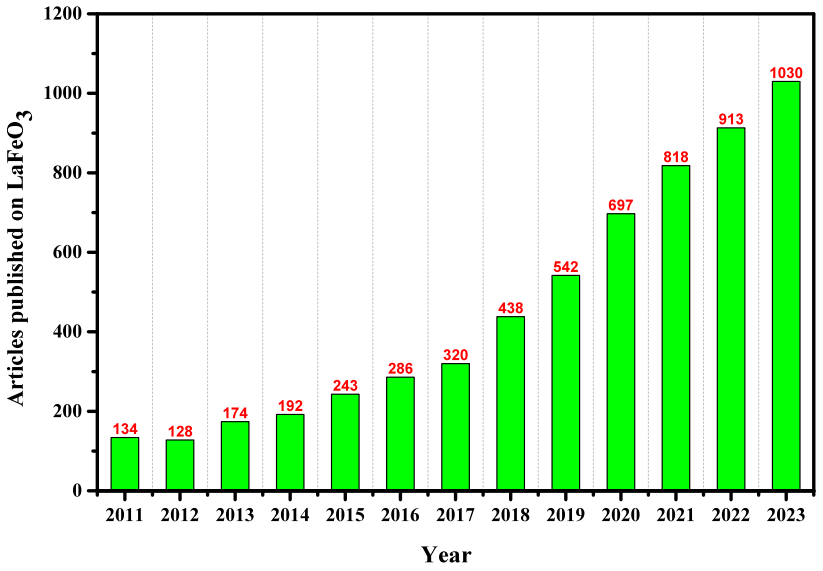

Figure 4. Number of research articles published on $LaFeO_3$ as a gas sensor.

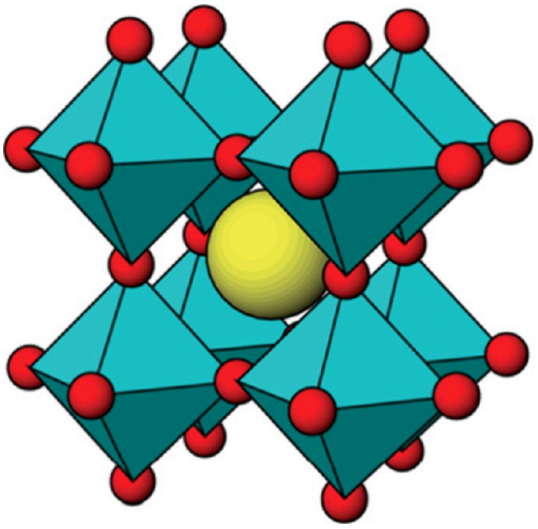

Figure 5. Image showing the crystal structure of ABX_3 perovskite. Reprinted from ref 35. Copyright 2012. American Chemical Society.

La sites with a small quantity of other elements results in variations in the adsorption of oxygen on the surface. Additionally, the replacement of Fe sites influences the characteristics of the adsorbents.[41] $LaFeO_3$ is a semiconductor material of p-type conductivity characterized by an orthorhombic crystal structure. The potential of heterojunctions formed between $LaFeO_3$ and n-type semiconductor materials for detecting a wide range of hazardous gases and volatile organic chemicals is considerable, particularly due to their ability to exhibit shorter response and recovery times. As a result, it exhibits favorable electronic and ionic conductivity, along with enhanced stability at relatively lower operating temperatures, as indicated by previous research.[41]

2. GAS SENSING MECHANISM OF $LaFeO_3$

Gas sensing techniques are commonly categorized into two distinct mechanisms. One category encompasses theories such as the Fermi level control theory, grain boundary barrier control theory, and electron depletion layer theory (EDL)/hole accumulation layer theory (HAL), which elucidate the alterations in electrical properties from a relatively microscopic standpoint. In every application, a change in electrical characteristics necessitates associated changes in physical characteristics such as energy bands and work functions.

The alternative theory focuses on the examination of the macroscopic interaction between materials and gases. This particular theoretical framework encompasses the adsorption−desorption model, the bulk resistance control mechanism, and the gas diffusion control mechanism.

These theories enable the utilization of modern material analysis tools that are grounded in apparent physical phenomena, thereby enhancing the efficiency and analyzing the process of gas sensing reactions. Figure 6 illustrates the schematic of plausible gas sensing.[41]

The operational principle of the $LaFeO_3$ gas sensor is based on the phenomenon of resistance change resulting from the adsorption and desorption of gas molecules on the surfaces of materials. The dominance of holes (h^+) as the primary charge carriers in $LaFeO_3$ can be attributed to its classification as a p-type semiconductor, where these holes are generated through the ionization of La^{3+} cation vacancies[42,43]

The sensor based on $LaFeO_3$ will undergo an initial reaction with oxygen present in the atmosphere due to the high electron affinity (0.43 eV). The oxygen molecules undergo adsorption on the surface of $LaFeO_3$, resulting in the formation of chemisorbed oxygen species (O_2^-, O^-, and O^2). The reaction during this process is as follows:

$$O_{2(gas)} \rightarrow O_{2(ads)} \quad (1)$$

$$O_{2(ads)} + e^- \rightarrow O^-_{2(ads)} \quad (2)$$

$$O^-_{2(ads)} + e^- \rightarrow 2O^-_{(ads)} \quad (3)$$

$$O^-_{(ads)} + e^- \rightarrow O^{2-}_{(ads)} \quad (4)$$

This process involves the transfer of electrons from the surface of $LaFeO_3$ to the oxygen species, leading to an increase in the concentration of holes (h^+) on the sensor's surface. The width of the hole accumulation layer on the surface of the $LaFeO_3$ sensor is altered either by an increase or reduction,

https://doi.org/10.1021/acsomega.4c00334
ACS Omega 2024, 9, 29994−30014

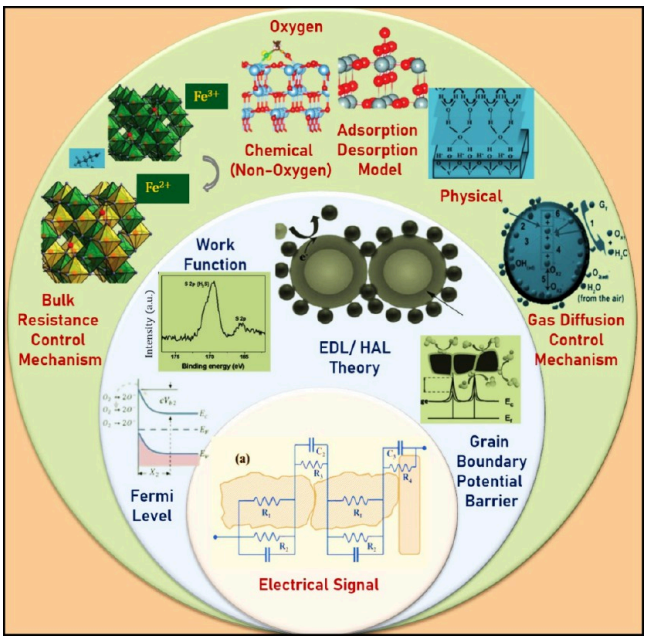

Figure 6. Gas sensing mechanism of sensors. Reproduced from ref 41. Copyright 2019, with permission from The Royal Society of Chemistry.

depending on the specific gas type, due to the reaction occurring between the gas molecules and the oxygen species that are adsorbed on the sensor's surface as shown in Figure 7, whereas Figure 8 depicts the list of reducing and oxidizing gases sensed by $LaFeO_3$.

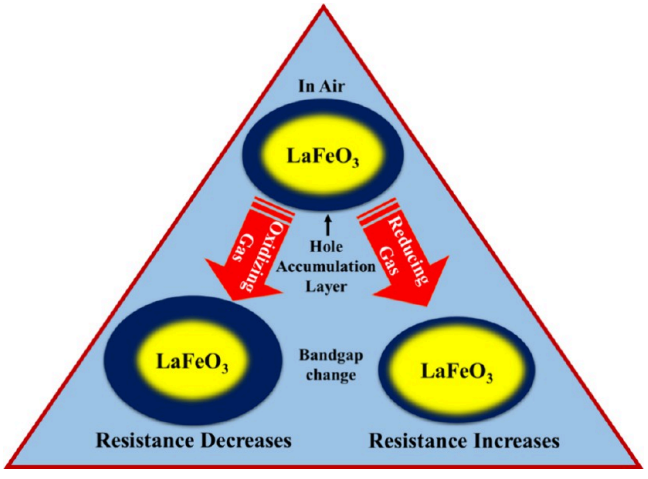

Figure 7. Gas sensing mechanism of $LaFeO_3$.

3. $LaFeO_3$ SYNTHESIS STRATEGIES

Gas sensing is a surface dependent property of a material. It is highly dependent on the surface morphology, porosity, particle size, as well as surface to volume ratio of the material. Hence the synthesis method can directly affect the gas-sensing ability of the material. At present, various methodologies have been documented in the literature pertaining to the synthesis of $LaFeO_3$ perovskites. A variety of techniques have been employed to generate captivating morphologies. Figure 9 illustrates the various routes for synthesizing $LaFeO_3$ perovskites. Lanthanum nitrate ($La(NO_3)_3{\cdot}6H_2O$) and ferric nitrate

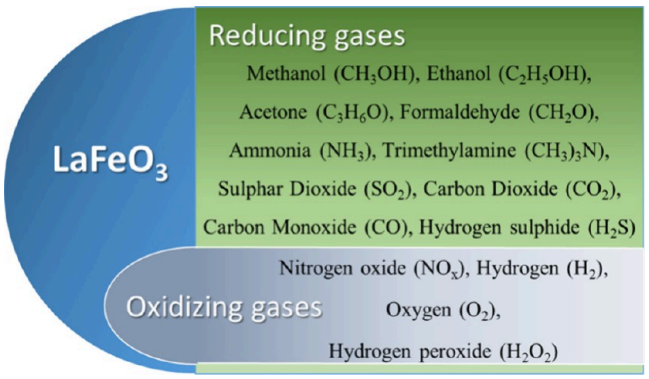

Figure 8. List of reducing and oxidizing gases sensed by $LaFeO_3$.

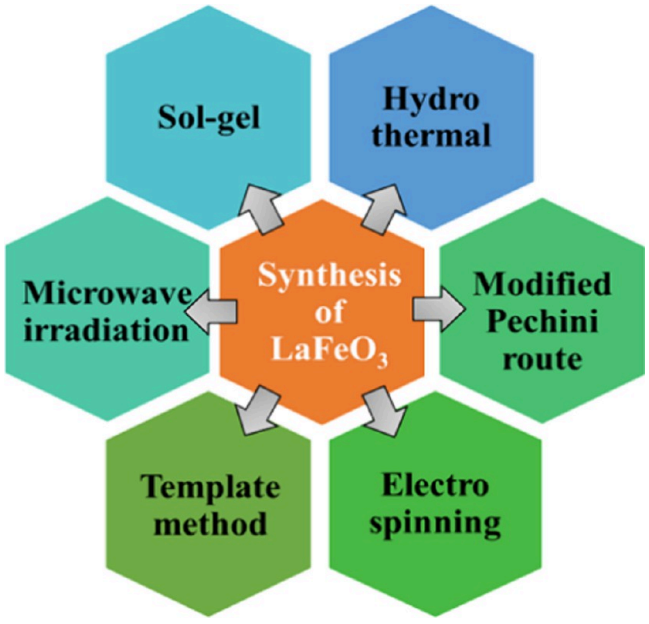

Figure 9. Various routes of synthesizing $LaFeO_3$ perovskites.

$(Fe(NO_3)_3{\cdot}9H_2O)$ are commonly employed as precursor materials in the synthesis of $LaFeO_3$. The impact of reaction conditions, such as temperature and reaction time, on the synthesis process can significantly influence the surface morphology and particle size.[33,44−53] The advantages and drawbacks of various techniques of synthesis of $LaFeO_3$ are listed in Table 1.

3.1. Hydrothermal Growth. Several authors have reported the synthesis of $LaFeO_3$ by a hydrothermal route. It is a simple and cost-effective method which produces nanocrystalline materials at a relatively low temperature with increased chemical reactivity. These advantages may be the reason for adopting the hydrothermal route by several researchers for the synthesis of $LaFeO_3$.[44,54−62]

In this technique, a sealed container known as an autoclave is used to perform a reaction where autogenous pressure is produced at an elevated temperature as shown in Figure 10. Autogenous pressure inside the autoclave depends on the temperature and fill factor, which is the ratio of volume of solution to available volume inside the autoclave. Controlled synthesis of $LaFeO_3$ is possible by varying the hydrothermal conditions. The reaction time of 6, 12, 18, and 24 h at 180 °C is responsible for developing the microspheres having crystallite size of samples about 59, 64, 76, and 88 nm,

https://doi.org/10.1021/acsomega.4c00334
ACS Omega 2024, 9, 29994−30014

Table 1. $LaFeO_3$ Synthesis Techniques with Advantages and Drawback

sr. no.	$LaFeO_3$ synthesis method	advantages	drawbacks	ref
1	**Citrate sol–gel**	Very low (10 nm) crystallite can be prepared.	It requires a high temperature for synthesis.	42
2	**Hydrothermal** 180 °C (10 h) (40 mL in 50 mL capacity Teflon lined autoclave)	Controlled size, low temperature growth, cost effective, and less complicated	Toxic byproducts can be produced.	43
3	**Hydrothermal with chemical etching** 140 °C (12 h)	Yolk-shell structure, the thin shell has good permeability to allow the diffusion of gas. The core and the outer and inner shells can provide a larger surface areas to absorb more target gas molecules.		44
4	**Electrospinning**	Efficient preparation of nanofibers of various morphology having a controlled size.	In the preparation of organic NFs, the variety of polymers used in electrospinning is limited.	33, 69–71
5	**Carbon sphere template method**	Provides enhanced surface activities, high surface-to-volume ratio, and fast diffusion, which allows easy gas penetration into the sensing layers.	It can only form an ordered mesoscopic structure.	45, 72
7	**PPMA template method**	Can effectively control the morphology, particle size, and structure during the preparation of nanomaterials		64
8	**Self-templated chemical process**	Hollow nanostructures, attributed with a large specific surface area and abundant paths for effective gas diffusion and reaction	Limited to small scale synthesis	48, 73
9	**Sol gel**	This process produces powders with a controlled size and shape and higher structure homogeneity, while the ratio of oxidization is lower, thanks to a low temperature procedure	Slow processing, cost and low amount of product	49
10	**Modified pechini route**	Good control over the structure and kinetics of the process, and the fine control of the product's chemical composition	High temperature method	50, 74
11	**Sol gel method based on PVA**	high purity, high crystallinity, narrow particle size distribution	Slow processing, cost and low amount of product	51, 75
12	**Rapid decomposition of the $La[Fe(CN)_6]\cdot 5H_2O$ under microwave irradiation**	high purity and short reaction time	It requires high electricity.	52

respectively, which can be calculated by using the Scherrer formula.[43,44] So just by increasing or decreasing the reaction time, the $LaFeO_3$ particles with required crystallite size can be developed easily through the hydrothermal method. The sample prepared by this technique exhibits spherical morphology with a high surface to volume ratio.

3.2. Sol–Gel Synthesis. Several researchers have adopted the sol–gel technique for the synthesis of $LaFeO_3$ and its composites as the synthesis of nanomaterials can be done easily with controlled parameters. Also this synthesis route requires a low reaction temperature and time compared to the hydrothermal method. Figure 11 explains the sol–gel process for the synthesis of $LaFeO_3$.[42,49]

At the beginning, all aqueous solutions of precursors with appropriate molar ratios will be mixed together and stirred by a magnetic stirrer to achieve a sol. On heating about 2–4 h, the sol turned into a highly viscous gel form, and further heating a gel burnt with violent combustion resulted in the powder in a loose form. Then the calcination is required to get the pure form of the sample. Doping and making different compositions of $LaFeO_3$ are also possible through this method.

It is observed that the $LaFeO_3$ samples prepared by the sol–gel method exhibited a spherical stonelike morphology, and the number of pores on the surface of samples prepared by the sol–gel method were greater than that of samples prepared by some other method.[63] Hence, $LaFeO_3$ prepared by the sol–gel method shows better sensitivity for many test gases than prepared by other methods.[63]

3.3. Other Methods for Synthesis of $LaFeO_3$. Qin et al.[64] reported the synthesis of $LaFeO_3$ by the PMMA (poly methyl methacrylate) method. PMMA colloidal crystals were added into the solution of precursors prepared in ethylene glycol and methanol and soaked for 3 h. Finally, by using vacuum filtration, excess solution was removed and dried. The prepared sample was calcined at 600 °C for 4 h, and a pure phase orthorhombic structure of $LaFeO_3$ with crystallite size 50 nm was obtained and confirmed by XRD analysis. SEM images revealed that PMMA crystals were eliminated completely by calcinations at 600 °C, and the ordered hexagonal arrangement of the inverse opal nanostructure was obtained as shown in Figure 12(a). The surface area and pore volume of samples were 24.907 m^2/g and 0.181 cm^3/g, respectively. The samples were tested for gas sensing for 100 ppm concentration of test gas; the obtained results are as shown in Figure 12(b) and the observed best sensitivity for methanol sensing, where the gas response value was 96.

Zhang et al.[45] reported the synthesis of $LaFeO_3$ hollow nanospheres using carbon spheres as a template. The process of synthesis of these hollow-nanospheres using carbon spheres as a template is illustrated in Figure 13. The carbanions spheres were obtained by keeping a glucose solution at 180 °C for 6 h in a hydrothermal autoclave followed by washing with distilled water and ethanol. These carbanion spheres were dispersed into the initial precursor of $LaFeO_3$ and heated for 24 h at room temperature. Finally the obtained $LaFeO_3$ powder calcined at 700 °C for 3 h. Nanospheres with a diameter of 300 nm were obtained. Zhang et al. concluded that hollow structures with an increased surface area will be favorable for application of gas sensors which exhibits a high response, good selectivity, and stability to formaldehyde gas.

Koonsaeng et al.[65] reported thermal decomposition of metal organic complex for the synthesis of a Sr doped $LaFeO_3$ metal organic complex by mixing of precursors and TEA with various

https://doi.org/10.1021/acsomega.4c00334
ACS Omega 2024, 9, 29994–30014

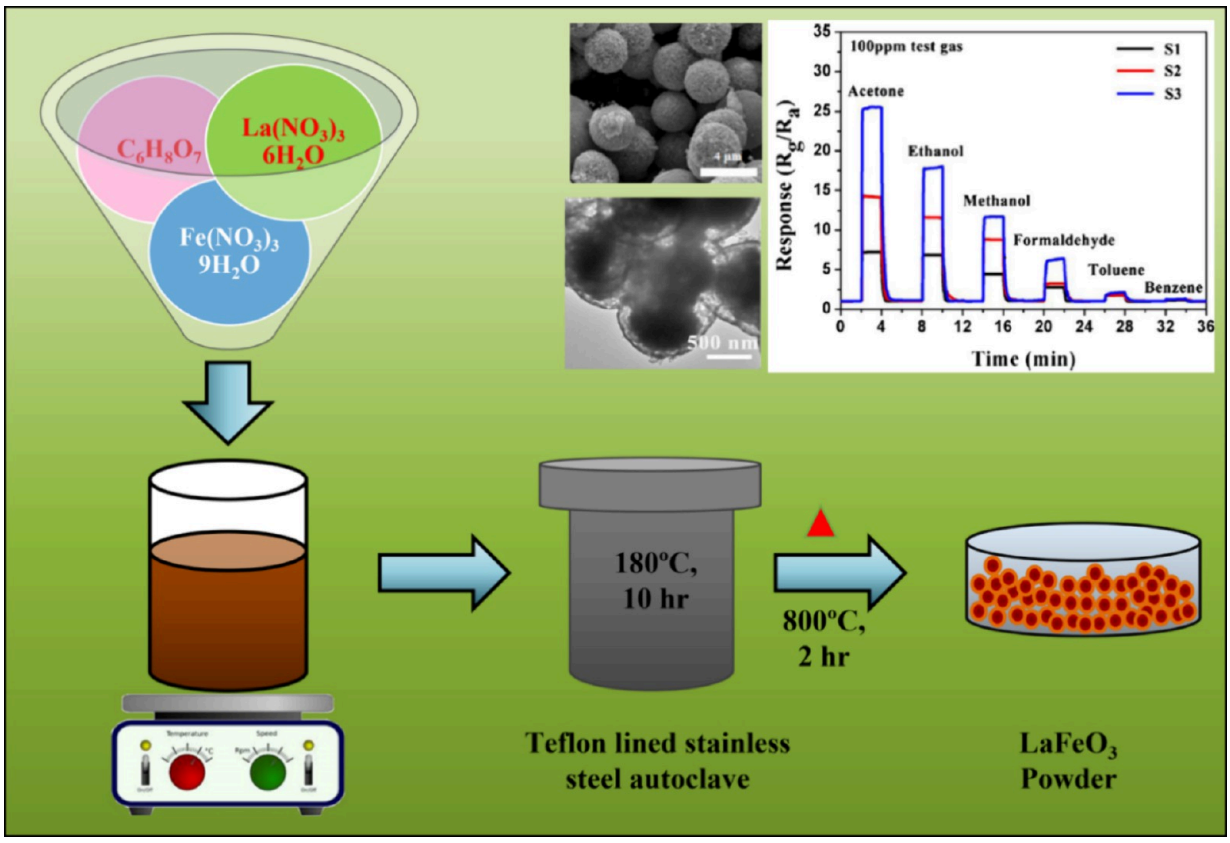

Figure 10. Hydrothermal synthesis process of $LaFeO_3$. Reproduced from ref 43. Copyright 2015 Elsevier and ref 44. Copyright 2018, with permission from Elsevier.

molar ratios in separated round-bottom flask which contained EG solvent and then distilled for 6 h at 190 °C with continuous stirring. Orthorhombic structure of prepared samples with grain size 2−5 μm and specific surface area 8−12 m^2/g was observed. The synthesized material showed good selectivity for ethanol having the highest response 31.8 at 350 °C for 100 ppm of ethanol concentration.

Zhang et al.[48] reported a precipitation method for synthesis of hollow spindles of $LaFeO_3$. Figure 14 shows the steps of the synthesis of the samples. These hollow spindles are then used for gas sensing. Compared to NH_3, SO_2, and CO samples, it shows good sensitivity for NO_2 at an operating temperature of 155 °C.

Matei et al.[66] reported the solution combustion synthesis of $LaFeO_3$. The solution combustion synthesis is a very famous, cheap, and nontoxic way to synthesize $LaFeO_3$ powders. Bellakki et al.[67,68] reported potassium doping up to 30% of $LaFeO_3$ by the combustion method.

Fan et al.[33] and Wei et al.[46] used an electrospinning technique for the synthesis of $LaFeO_3$. The width and thickness of prepared nano belts/nanowires were controlled by varying parameters. The synthesis process is shown in Figure 15.

4. $LaFeO_3$ FOR REDUCING GASES SENSING

4.1. Acetone (C_3H_6O) Sensing. Acetone is a volatile organic compound, widely used in industry, laboratory, medical fields, and domestic applications. The flammable nature of acetone makes it most hazardous. Hence, there is a need to develop sensors that detect acetone vapors accurately and rapidly.

Chen et al.[76] reported the acetone sensing mechanism with $LaFeO_3$ as a sensor. Acetone releases electrons from preadsorbed oxygen species to the $LaFeO_3$ surface that causes a change in resistance of $LaFeO_3$. Molecules of acetone can react with O^- and O^{2-} ions in two ways: (a) adsorbs on O^- ions or (b) replaces weakly adsorbed O^{2-} on the Fe site, with the formation of an oxygen molecule (eq 5). They have used a sol−gel route for the synthesis of $LaFeO_3$ powder, and the prepared powder was annealed in an oven (4 h) at different temperatures such as 700 °C, 800 °C, 900 °C, and 1000 °C. It was observed that the resistance of prepared samples in air varies with its annealing temperature (Figure 16). The resistance value decreases with an increase in the annealing temperature.

The prepared powder samples are then coated by making its paste with deionized water onto an alumina tube (4 mm in length and 1.2 mm in diameter) about 250 μm thick. This was further heated for 48 h for 240 °C and used for gas sensing. During the gas sensing study, it is observed that the sample annealed at 800 °C shows excellent acetone sensing properties at 260 °C with a response time of 62 s and a recovery time of 107 s. Hence, the sensitivity of $LaFeO_3$ is highly influenced by the annealing temperature as well as by the operating temperature.

$$CH_3COCH_3 + 8O^-_{(ads)} \rightarrow 3CO_2 + 3H_2O + 8e^- \quad (5)$$

Xiao et al.[43] reported that possible mechanisms of formation of porous $LaFeO_3$ microspheres were explained through the Ostwald Ripening process and its acetone sensing property. $LaFeO_3$ microspheres were prepared by the hydrothermal method using a Teflon lined autoclave of 50 mL capacity at

https://doi.org/10.1021/acsomega.4c00334
ACS Omega 2024, 9, 29994−30014

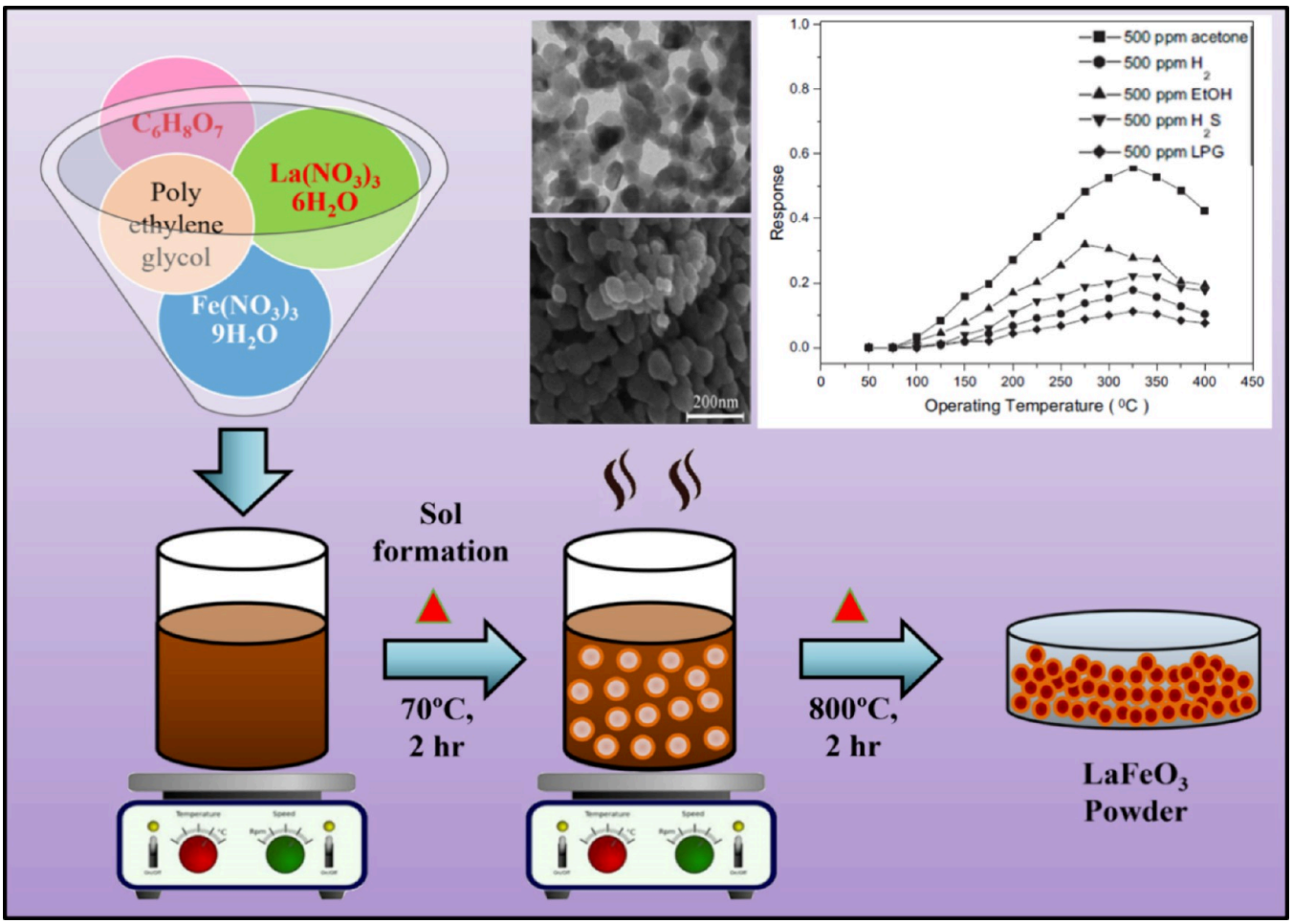

Figure 11. Sol–gel process for the synthesis of $LaFeO_3$. Reproduced from ref 42. Copyright 2011 Elsevier and ref 49. Copyright 2017, with permission from Elsevier.

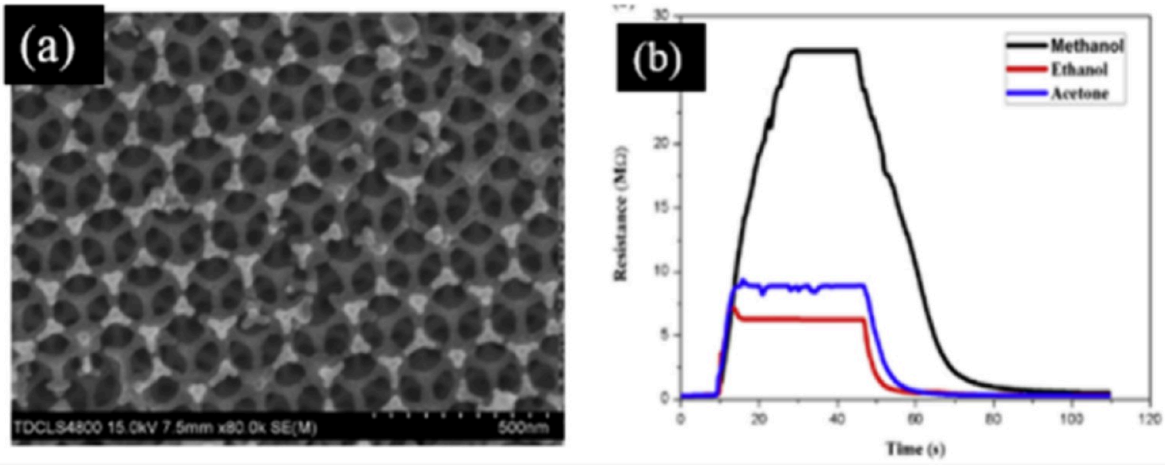

Figure 12. (a) SEM image of $LaFeO_3$ synthesized by the PMMA method and (b) its gas sensing performance. Reproduced from ref 64. Copyright 2015, with permission from Elsevier.

180 °C for 10 h, and prepared samples were calcined at 800 °C for 2 h. Oriented attachment and a self-assembly mechanism caused the formation of porous $LaFeO_3$ microspheres. Figure 17 shows (a) low-magnification and (b) high-magnification SEM images of as-prepared $LaFeO_3$ microspheres.

These porous microspheres were mixed with water to form a paste, which was coated onto an alumina tube (7 mm in length and 1.5 mm diameter) having gold electrodes at both ends for testing gas sensing performance. It was observed that these microspheres exhibit excellent performance to acetone.[43]

Murade et al.[42] reported the synthesis of Sr-doped nanostructured $LaFeO_3$ and its acetone sensing performance. $La_{1-x}Sr_xFeO_3$ (x = 0, 0.1, 0.2, 0.3, and 0.4) was prepared by using a sol–gel citrate method, and the sensor was fabricated

https://doi.org/10.1021/acsomega.4c00334
ACS Omega 2024, 9, 29994–30014

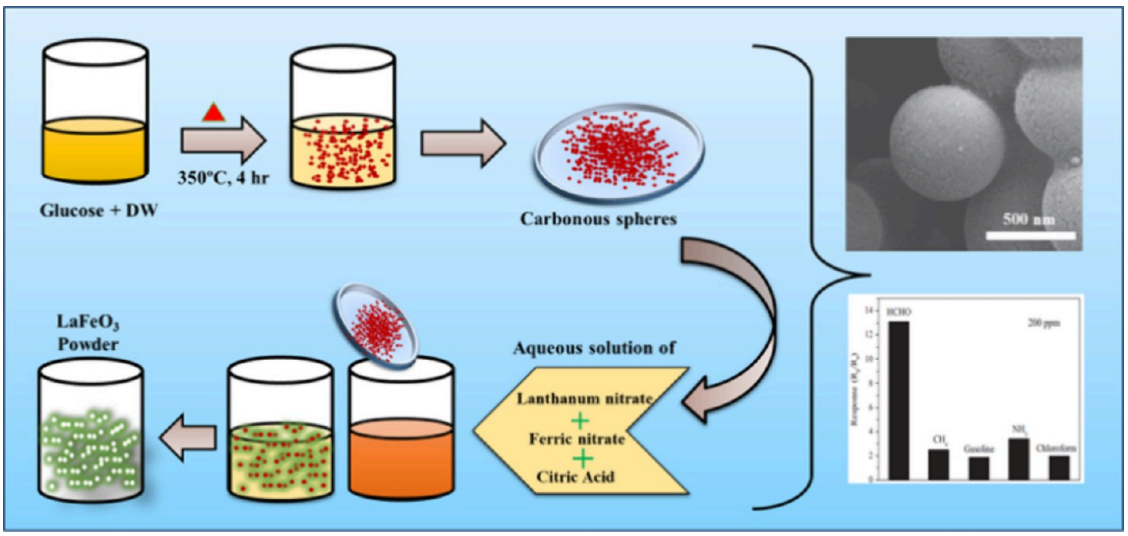

Figure 13. Carbon sphere template method for the synthesis of $LaFeO_3$ and its SEM image and gas sensing performance. Reproduced from ref 45. Copyright 2014, with permission from Elsevier.

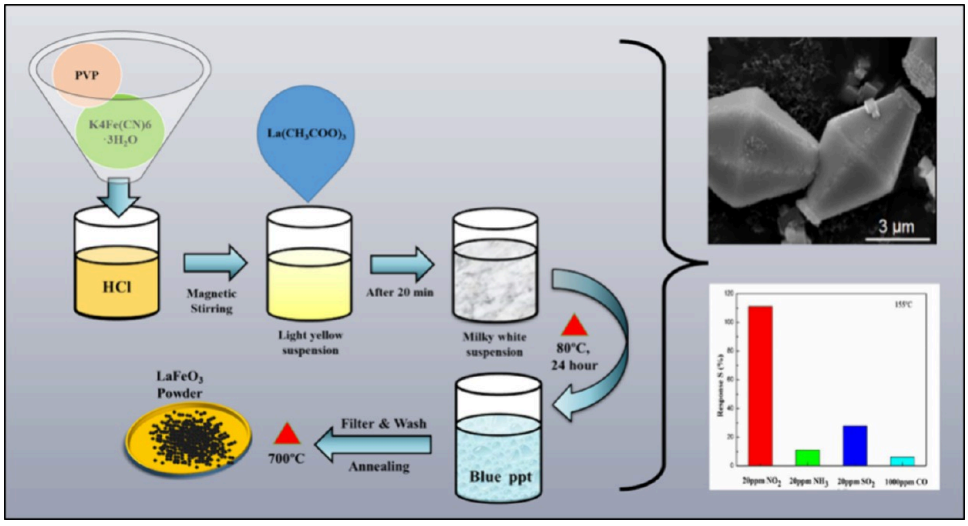

Figure 14. Precipitation method for synthesis of hollow spindles of $LaFeO_3$, its SEM images, and gas sensing performance. Reproduced from ref 45. Copyright 2014, with permission from Elsevier.

by coating a thick film of prepared power on a ceramic tube which was printed with a Au electrode and Pt conducting wires. It clearly indicated that $La_{0.7}Sr_{0.3}FeO_3$ shows good response to acetone at 275 °C. The summary of results of acetone sensing by $LaFeO_3$ is shown in Table 2.

4.2. Ethanol (C_2H_5OH) Sensing. Ethanol (ethyl alcohol) is a flammable and volatile organic compound and mainly used as a fuel in engines, rockets, fuel cells, and also household heating/cooking. Also, ethanol has applications in the medical field. Ethanol sensors are more popular and in great demand due to the highly flammable nature of ethanol. Many researchers reported $LaFeO_3$ and its compounds for ethanol sensing. The summary of the results of ethanol sensing by $LaFeO_3$ is shown in Table 3.

Reaction:

$$C_2H_5OH + 6O^{n}_{(ads)} \rightarrow 2CO_2 + 3H_2O + 6ne^{-} \quad (6)$$

Song et al.[78] reported a Pb doped $LaFeO_3$ ethanol sensor with enhanced sensitivity. They prepared nanocrystalline $La_{1-x}Pb_xO_3$ (x = 0, 0.1, 0.2, 0.3) material using the sol−gel method. The XRD pattern of prepared samples showed a perovskite phase with orthorhombic structure. With the increasing value of x, the unit cell volume should be increased because the Pb^{2+} ion is larger than replaced La^{3+} ions, but when the value of x exceeds 0.3, the cell volume decreased due to stoichiometric structure of $LaFeO_3$ perovskite transformed into the nonstoichiometric $La_{1-x}Pb_xO_3$ structure. The crystallite grain size decreased with the increase in Pb content that indicated Pb doping can restrain the growth of the grain size. To study gas sensing performances the slurry of prepared samples using PVA as a binder is coated on the Al_2O_3 tube having a length of 8 mm, external diameter of 2 mm, and internal diameter of 1.6 mm, and it was calcined 2 h at 400 °C. It was tested for gas sensing, the results of gas sensing at 500 ppm for various test gases shown in Figure 18. It is clear that Pb doping is beneficial for the performance of ethanol sensing, and the maximum sensitivity is achieved at x = 0.2 for an operating temperature of 140 °C (Figure 18).

Koonsaeng et al.[65] reported the Sr doped $LaFeO_3$ as a promising candidate for ethanol detection. Sr doped $LaFeO_3$

https://doi.org/10.1021/acsomega.4c00334
ACS Omega 2024, 9, 29994−30014

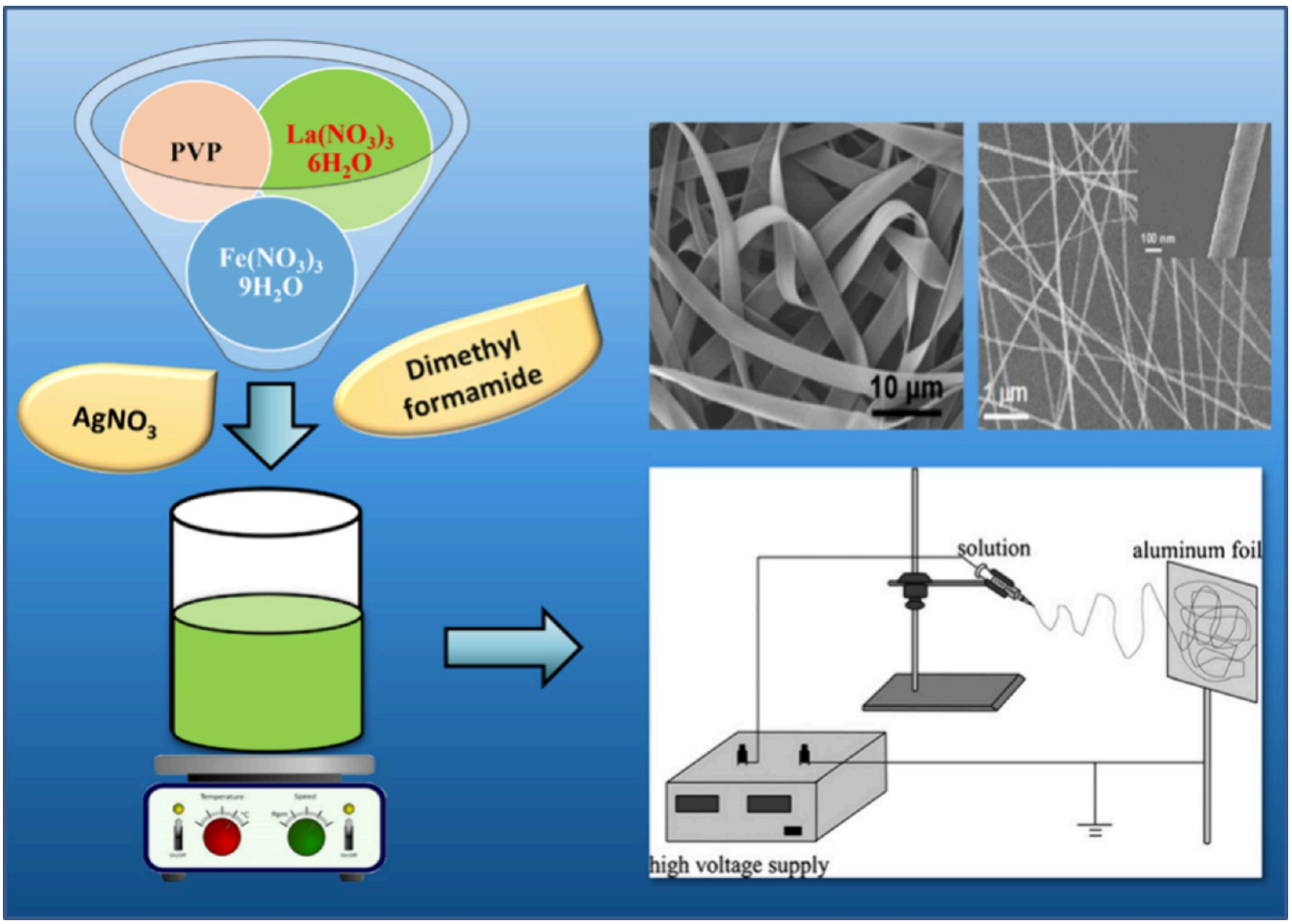

Figure 15. Electrospinning technique for the synthesis of $LaFeO_3$ and its SEM images. Reproduced from ref 33. Copyright 2011 Elsevier and ref 46 copyright 2017, with permission from Elsevier.

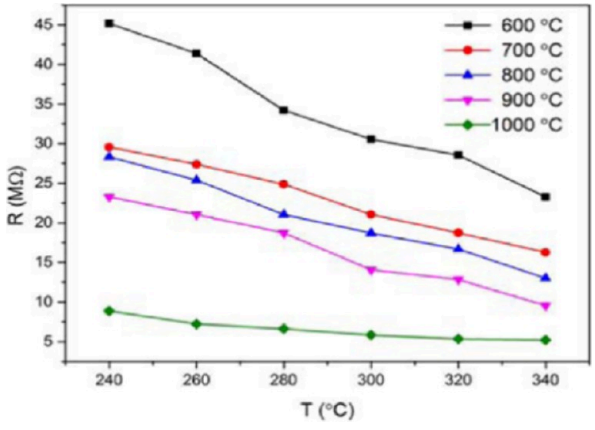

Figure 16. Resistance of samples in air with annealing temperature. Reprinted from ref 76. Copyright 2016, with permission from Elsevier.

was prepared by thermal decomposition of the metal organic d-complex as follows. First of all, precursors and TEA were mixed with appropriate molar ratios in a round-bottom flask which contains EG solvent and distilled at 190 °C for 6 h. The obtained precipitate was washed, dried, and calcined at 850 °C for 4 h. The phase formation is confirmed from the XRD analysis (Figure 19). The paste of the prepared sample was coated onto an alumina substrate 3 mm in length and 2 mm in

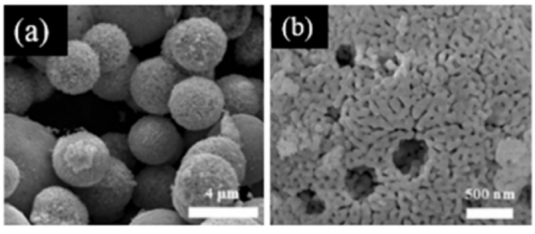

Figure 17. (a) Low-magnification and (b) high-magnification SEM images of $LaFeO_3$ microspheres. Reprinted from ref 43. Copyright 2015, with permission from Elsevier.

width which is formed by using X-100 binder and acetyl acetone as a solvent. Gold electrodes were fixed at the both ends of the substrate. Further it was annealed at 400 °C to become ready for a gas sensing study. The gas sensing properties of $La_{1-x}Sr_xO_3$ were studied for some reducing gases including ethanol, acetone CH_4, H_2 in the range of an operating temperature of 200−300 °C. The highest sensitivity for ethanol gas was observed due to active sites for ethanol adsorption which were generated because of the substitution of La^{3+} with Sr^{2+} ionic dopants. The maximum response for ethanol was 31 with a short response and recovery time as recorded at 350 °C.

Wang et al.[32] achieved a stable sensing performance to ethanol by a $BaTiO_3/LaFeO_3$ sensor at operating temperature

https://doi.org/10.1021/acsomega.4c00334
ACS Omega 2024, 9, 29994−30014

Table 2. Acetone Sensing Performance of $LaFeO_3$

material	method	doping	sensitivity	formula	time response/ recovery (s)	operating temp (°C)	ref
$LaFeO_3$	Sol–gel citrate	Sr x = 0.3 ($La_{1-x}Sr_xFeO_3$)	0.8 @ 500 ppm	$S = (R_a-R_g)/R_a$	20/270	275	42
α-Fe_2O_3 /$LaFeO_3$ heterojunction	Hydrothermal method 180 °C	α-Fe_2O_3	48.3 @ 100 ppm	$S = R_g/R_a$	16.5/2	350	34
$LaFeO_3$	Sol–gel annealed at 800 °C	—	2.068 @ 0.5 ppm	$S = R_g/R_a$	62/107	260	76
$LaFeO_3$	Hydrothermal method 180 °C for 10 h	—	14.2 @ 50 ppm	$S = R_g/R_a$	9/17	260	43
$LaFeO_3$	Sorghum straw as biotemplate	—	12.4 @ 200 ppm	$S = R_g/R_a$	9/18	240	77
Yolk-shell $LaFeO_3$ microspheres	Hydrothermal method combined with annealing and etching process		25.5 @ 100 ppm	$S = R_g/R_a$	5/25	225	44

Table 3. Ethanol Sensing Performance of $LaFeO_3$

material	method	doping	sensitivity	formula	time response/ recovery (s)	operating temp (°C)	ref
$La_{1-x}Pb_xFeO_3$	Sol–gel at 60 °C	Pb	14 @100 ppm (x = 0.2)	R_g/R_a	10/40	140	78
$La_{0.75}Ba_{0.25}FeO_3$	Sol–gel	Ba	3.8	R_g/R_a	10/14	240	81
			2.4 @10 ppm		17/25		
$LaFeO_3$	Thermal decomposition of metal organic complex	Sr	31.8 @1000 ppm ($La_{0.5}Sr_{0.5}FeO_3$)	R_g/R_a	120	350	65
$BaTiO_3/LaFeO_3$	Citric sol–gel method	$BaTiO_3$ /$LaFeO_3$ (ratio 1:2)	102.7 @100 ppm	R_g/R_a	16	128	32
$LaFeO_3$	Hydrothermal method (annealing and etching)	Yolk shell	3.8 and 6.7 @100 ppm	$S = R_g/R_a$	5/25	225	44
$LaFe_{1-x}Mn_xO_3$	Sol–gel method	Mn (x = 0, 0.2, 0.3, 0.5, 0.6)	1.62 @50 ppm	$S = R_a/R_g$	23/31	210	79
$LaFeO_3$-Fe_2O_3	Electrospinning	—	8.9	$S = R_g/R_a$	150/250	170	33
			4.9 @ 500 ppm		10/24	285	
$LaFe_xO_{3-\delta}$	Sol–gel	x = 0.7/ 0.8/0.9/1.0/1.1/1.2/1.3	132 @ 1000 ppm	$S = R_g/R_a$	1/1.5	140	80

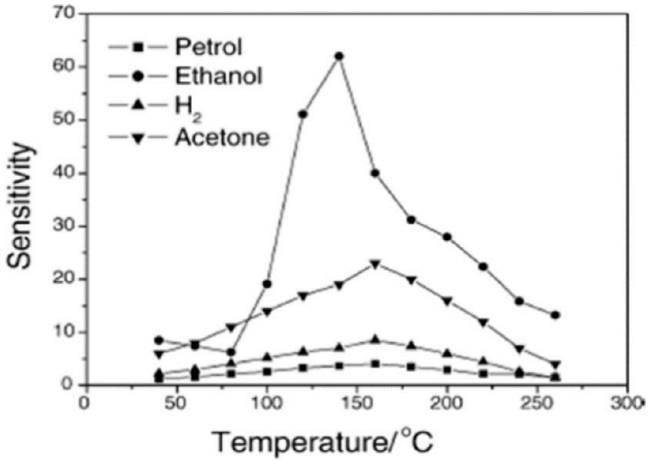

Figure 18. Graph of sensitivity vs operating temperature. Reprinted from ref 78. Copyright 2005, with permission from Elsevier.

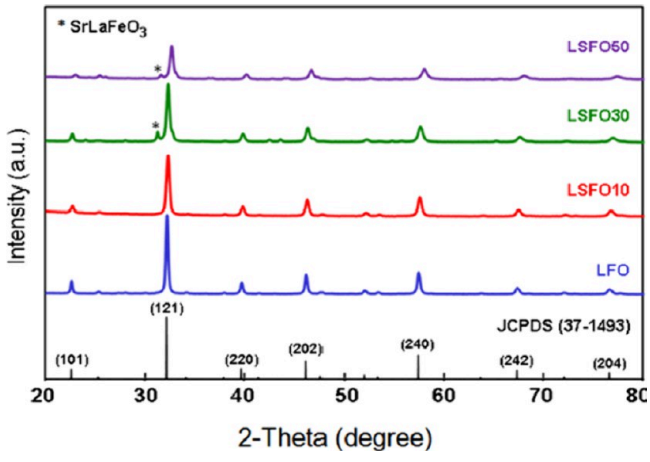

Figure 19. XRD pattern of $LaFeO_3$ and Sr doped $LaFeO_3$. Reprinted from ref 76. Copyright 2018 Elsevier.

128 °C. To prepare a $BaTiO_3/LaFeO_3$ nanocomposite, $BaTiO_3$ nanoparticles and $LaFeO_3$ nanoparticles were mixed in a molar ratio of 1:2 and calcined for 2 h at 200 °C. These $BaTiO_3/LaFeO_3$ prepared nanocomposite powder was mixed with terpineol to form a paste, and its thin film was coated onto a ceramic tube (outer diameter 1.2 mm, length 4 mm) which was preinstalled with gold electrodes at its two ends. After annealing at 600 °C it was used for the gas sensing study. The $BaTiO_3/LaFeO_3$ sensor exhibit improved the capability of absorbing the oxygen species in air and show a dynamic response to ethanol as shown in Figure 20.

Fan et al.[33] reported formation of $LaFeO_3$-Fe_2O_3 nanobelts as a promising candidate for ethanol detection by electrospinning. The width and thickness of prepared nanobelts are measured in SEM as shown in Figure 21. The gas sensing performance was investigated by coating these nanobelts onto a ceramic tube (diameter 1.35 mm and length 4 mm having predeposited gold electrodes) for different gases, and in

https://doi.org/10.1021/acsomega.4c00334
ACS Omega 2024, 9, 29994–30014

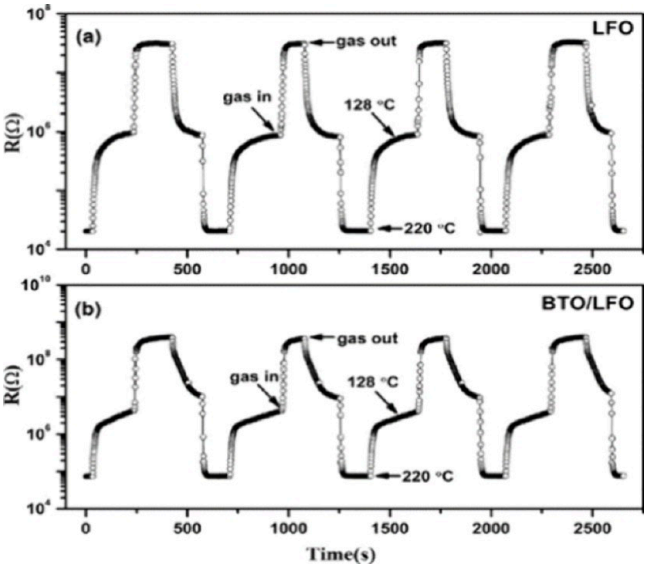

Figure 20. Ethanol sensing by (a) $LaFeO_3$ and (b) $BaTiO_3/LaFeO_3$. Reprinted from ref 32. Copyright 2019, with permission from Elsevier.

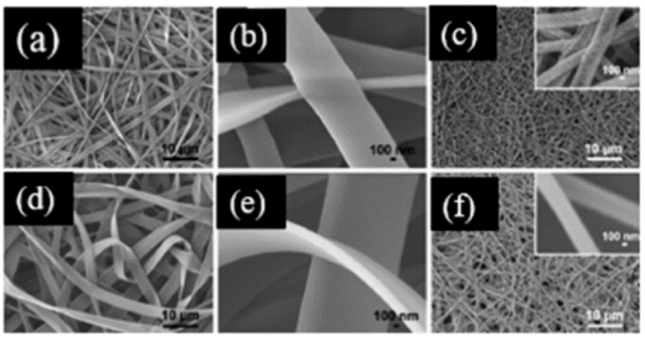

Figure 21. (a) Low-magnification and (b) high-magnification SEM images of untreated $Fe(NO_3)_3$-PVP composite nanobelts. (c) SEM image of the Fe_2O_3 composite nanobelts calcined at 600 °C (inset: magnified image). (d) Low-magnification and (e) high-magnification SEM images of untreated $La(NO_3)_3$-$Fe(NO_3)_3$-PVP composite nanobelts. (f) SEM image of $LaFeO_3$ composite nanobelts calcined at 600 °C (inset: magnified image). Reprinted from ref 33. Copyright 2011, with permission from Elsevier.

conclusion it is declared that $LaFeO_3$-Fe_2O_3 nanobelts are the more suitable as a sensing material for ethanol gas.

Li et al.[79] reported n-type $LaFe_{1-x}Mn_xO_3$ for ethanol sensing and explained transformation of a p-type $LaFeO_3$ to n-type $LaFe_{1-x}Mn_xO_3$ semiconductor. Lanthanum nitrate, ferric nitrate, and citric acid were dissolved in 25 mL of distilled water, and subsequently, Mn-nitrate was added dropwise and stirred for 30 min. Then 0.5 g of PEG was added, and an orange-red wet gel was formed. Again, the wet gel was dried at 80 °C for 10 h to obtain a dry gel (powder). The prepared powder was calcinated at 700 °C for 3 h, and gas sensing performance was observed by coating a 60-μm-thick film of prepared powder onto a ceramic tube that was 4 mm in length, 1.2 mm external diameter, and 0.8 mm internal diameter. Typically, the $LaFeO_3$ semiconductor shows a p-type nature that when it was exposed to a reducing gas its resistance value increased rapidly. But due to the doping of Mn, structural defects were formed, electronic compensation was dominant, and the material showed behavior of an n-type semiconductor. In the presence of reducing gas, the acetone resistance of the prepared samples decreased rapidly and acted as an n-type semiconductor ethanol sensor.

Cao et al.[80] prepared nanocrystalline $LaFe_xO_{3-\delta}$ powder by the sol–gel method with x = 0.7/0.8/0.9/1.0/1.1/1.2/1.3. To fabricate the gas sensing device, prepared nanocrystalline $LaFe_xO_{3-\delta}$ powder was coated onto a ceramic tube having an outer diameter of 1.2 mm and length of 4 mm, which is preinstalled with gold electrodes. $LaFe_{0.8}O_{3-\delta}$ shows the best sensitivity for ethanol sensing due to its relatively large surface concentration of adsorbed oxygen species and monodentate La-carbonate.

4.3. Methanol (CH_3OH) Sensing. Rong et al.[47] reported cage and core–shell structures of Ag doped $LaFeO_3$ which showed excellent performance toward methanol sensing. These structures were developed by using the molecular imprinting technique. Its structural and morphological properties were studied by XRD, SEM, TEM, and FTIR. Figure 22(a) and (c)

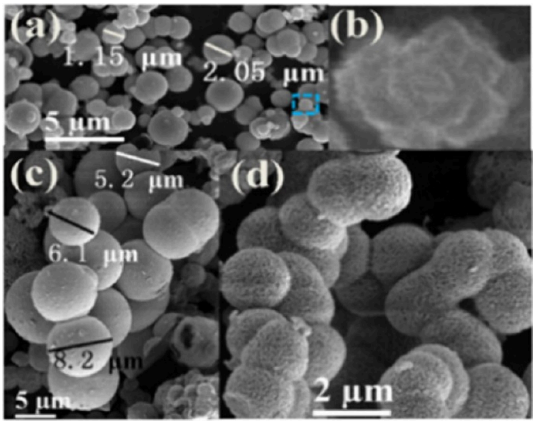

Figure 22. (a) and (c) Low-magnification SEM images of as-prepared cage and core–shell samples; (b, d) high-magnification images of cage and core–shell samples. Reprinted from ref 47. Copyright 2018, with permission from Nanotechnology, IOP Publishing.

shows low-magnification SEM images of as-prepared cage and core–shell samples, and Figure 22(b) and (d) shows high-magnification images of cage and core–shell samples. To perform gas sensing analysis, the paste of as-synthesized samples was coated onto the outside of an alumina tube (4 mm in length, 1.2 mm in external diameter, and 0.8 mm in internal diameter) with electrode pair of Au at each end. The thickness of sample coatings on the tube is about 0.6–0.8 mm. The cage and core–shell exhibit 16.98 and 33.7 response values at 215 and 195 °C, respectively, for 5 ppm of methanol gas concentration.

$$CH_3OH_{(ads)} + 2O^{2-}_{(ads)} \rightarrow CO_2 + H_2O + 4e^- \quad (7)$$

Rong et al.[82] further developed graphene doped Ag-$LaFeO_3$ for the application of methanol sensing. Ag-$LaFeO_3$ modified with graphene showed very excellent performance for methanol sensing. The samples prepared by 0.75% weight ratios of graphene in $LaFeO_3$ have the best selectivity for methanol. At 5 ppm of methanol concentration, the sensor based on 0.75% graphene doped Ag-$LaFeO_3$ showed a response value about 51 at the operating temperature 102 °C. Hence, Ag-$LaFeO_3$ graphene exhibited an increased surface area compared to Ag-$LaFeO_3$.

https://doi.org/10.1021/acsomega.4c00334
ACS Omega 2024, 9, 29994–30014

Rong et al.[63] reported quasimolecular imprinted Ag-$LaFeO_3$ as an ultrasensitive methanol sensor. A sol−gel and combustion method was adopted for the synthesis of Ag doped $LaFeO_3$, and methanol was used as a solvent in fabrication of the methanol sensor. Use of methanol as a solvent offered a positive impact on the gas sensing properties of the device. The sample prepared by the sol−gel method is more sensitive to methanol than the sample prepared by the combustion technique because of the large number of pores formed on the surface of sample prepared by sol−gel method which can be clearly seen in the images by scanning electron microscopy (SEM) shown in Figure 23. This increased the number of pores and more sites to absorb the molecules of the test gas.

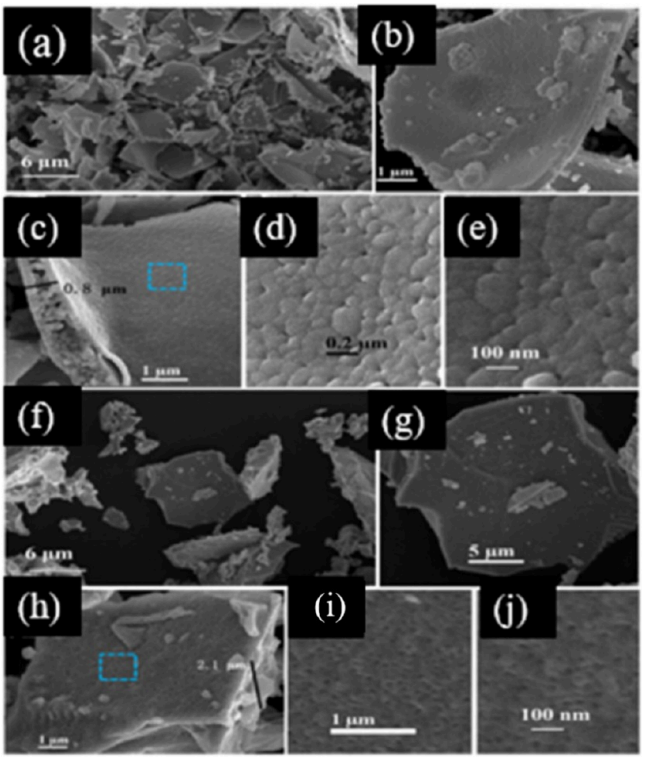

Figure 23. SEM images of Ag doped $LaFeO_3$ as-synthesized by (a, b, c, d, e) combustion and the sol−gel (f, g, h, i, j) method at various magnification levels. Reprinted from ref 63. Copyright 2018, with permission from Springer Nature.

Rong et al.[29] reported a heterojunction of Ag-$LaFeO_3$ with nitrogen doped carbon quantum dots as a methanol sensor. This heterojunction was an excellent candidate for the detection of methanol due to its improved electron transport and charge pair separation ability. In Ag-$LaFeO_3$/NCQDs a bridge between NCQDs and Ag-$LaFeO_3$ is formed for transport of charge, which carries electron transport easily. Hence it will reduce the response and recovery times of the sensor.

Qin et al.[64] synthesized microporous structured $LaFeO_3$ for methanol sensing. The spheres of monodispersed poly(methyl methacrylate) were used as a template to prepare the 3D-ordered macrospores. The morphology and structure were confirmed by XRD, SEM, and TEM techniques. The increased surface area of $LaFeO_3$ due to the ordered three-dimensional structures will highly influence the sensing property of material compared to bulk reference $LaFeO_3$. The 3D-ordered macrospores of $LaFeO_3$ exhibited both a microporous and mesoporous nature and caused Knudsen diffusion and molecular diffusion of gas, which largely affected the sensitivity of the material. Table 4 shows a summary of results of methanol sensing by $LaFeO_3$.

4.4. Formaldehyde (HCHO) Sensing. The use of formaldehyde is very common in various industries as well as in medical laboratories, and it is actually a pollutant in the indoor environment. $LaFeO_3$ is very sensitive for the detection of formaldehyde. Table 5 shows the summary of formaldehyde sensing results by $LaFeO_3$ based sensors.

Zhang et al.[45] reported formaldehyde sensing by $LaFeO_3$ hollow nanospheres. These nanospheres were synthesized successfully using carbon nanospheres as templates. First of all, carbon spheres were prepared by a hydrothermal method and then dispersed into the initial solution of precursors of $LaFeO_3$ edged at room temperature for 24 h. Then after centrifuge washing and drying in an oven, a powder was obtained, which was finally calcined at 700 °C. These prepared nanospheres were characterized by XRD and FESEM, and the gas sensing property was studied. To perform the gas sensing test, a paste of prepared powder samples in water was formed and printed as a 300 mm thick film on an alumina tube with 7 mm in length and 1.5 mm in diameter with predeposited Au electrodes at both ends of the tube. The results of gas sensing clearly showed that $LaFeO_3$ hollow nanospheres are the best material for formaldehyde sensing.

$$HCHO + 2O^{2-}_{(ads)} \rightarrow CO_2 + H_2O + 2e^- \quad (8)$$

Wei et al.[46] reported Ag doped $LaFeO_3$ as highly sensitive and fast formaldehyde gas sensor. Initially Ag doped $LaFeO_3$ and undoped $LaFeO_3$ nanofibers were synthesized by the electrospinning method, and the chemical and structural analysis was carried out using XRD, SEM, and HRTEM. The formaldehyde sensing of prepared samples was studied by coating a 300 μm thick film on a ceramic tube having Au electrodes connected through a Pt wire. It is found that $LaFeO_3$ detects a lower concentration of formaldehyde as compared to pristine $LaFeO_3$ material, and this is because the Ag in $LaFeO_3$ will promote the reaction rate by acting as a catalyst between surface adsorbed oxygen ions and formaldehyde gas molecules. During the doping of Ag, some Ag atoms replace the atoms of $LaFeO_3$ and formthe defects, which increased hole concentration in the material.

Zhang et al.[84] reported Ag-$LaFeO_3$ modified by SWCNT (single-walled carbon nanotubes) as an improved formaldehyde sensor. Initially Ag doped $LaFeO_3$ was prepared by the sol−gel method and further modified by single wall carbon nanotubes. The resistance of SWCNT-$LaFeO_3$ samples is comparatively lower than that of $LaFeO_3$ due to the easy transportation of electrons through SWNT which affects the operating temperature. As prepared 0.75% SWCNT is the optimal ratio to modify $LaFeO_3$, above the 1% of SWCNT agglomeration starts. This drastically affected the electron conductivity of sensing material which also depends on proportion of dopant below 1%. Due to decrease in resistance of sensor it can operate at low temperature. The reduction in operating temperature due to the doping of SWNT and well dispersed particles causes increase in specific surface area and increased number of adsorbing vacancies on the surface of sensor. To perform gas sensing test, paste of prepared powder

https://doi.org/10.1021/acsomega.4c00334
ACS Omega 2024, 9, 29994−30014

Table 4. Methanol Sensing Performance of $LaFeO_3$

material	method	doping	sensitivity	formula	time response/ recovery (s)	operating temp °C	ref
Ag-$LaFeO_3$	Sol−gel and microwave chemical synthesis	Graphene0.75 % weight percent	51 @5 ppm	R_g/R_a	30/28	102	82
Ag-$LaFeO_3$	Sol−gel (ALS) and combustion (ALC) synthesis quasi-molecular imprinting technology	Ag	(ALS) 52.29	R_g/R_a	32/37	155	63
			(ALC) 34.89 @ 5 ppm				
$LaFeO_3$	Sol−gel method combined with molecularly imprinted technology as precursors	Silver-doped	33.5 @ 5 ppm	R_g/R_a	42/57	195	47
Nitrogen-doped carbon quantum dot/Ag-$LaFeO_3$	Microwave synthesizing	Ag	73 @5 ppm	R_g/R_a		92	29
Ag-$LaFeO_3$ molecularly imprinted polymers (ALMIPs)	Sol−gel method molecularly imprinted (filter paper, silk and carbon fiber template)	Ag 0.1 mmol silver nitrate	23.5	R_g/R_a		175 (fiber 1)	83
			19.67			125 (fiber 2)	
			17.59 @ 5 ppm			125 (fiber 3)	
$LaFeO_3$	PMMA template method		96 @ 96−100 ppm	R_g/R_a	25/23	190	64

Table 5. Formaldehyde Sensing Performance of $LaFeO_3$

material	method	doping	sensitivity	formula	time response/ recovery (s)	operating temp (°C)	ref
Ag−$LaFeO_3$	Sol−gel method combined with the microwave chemical synthesis	SWCNTs 0.75% weight ratio	23	—	6/20	86 °C	84
			0.5				
$LaFeO_3$	Hydrothermal (180 °C)		13 @200 ppm	R_g/R_a		260 °C	45
$LaFeO_3$	Electro spinning method	Ag 10%	4.8 @5 ppm	R_g/R_a	2/4	230 °C	46
Ag-$LaFeO_3$	B, N, S, Cl doped graphene	Ag	For B = 18 @ 1 ppm	R_g/R_a	23/30	27 °C	85
Herichal microporous $LaFeO_3$	Sol−gel method	—	116 @50 ppm	R_g/R_a	90	125 °C	40

Table 6. NO_2 Sensing Performance of $LaFeO_3$

material	method	doping	sensitivity	formula	time response/recovery (s)	operating temp (°C)	ref
$LaFeO_3$	Hydrothermal	rGO	183.4% @3 ppm	$(R_a\text{-}R_g)/R_g \times 100$	—	250 °C	86
$LaFeO_3$	Radio frequency magnetron sputtering technique	—	29.60	$(R_a/R_g) \times 100$	24/35	RT (25)	87
			10.04 @1 ppm		30/42		
$LaFeO_3$	Self-templated chemical process	—	81.4% 5 ppm	$(R_a\text{-}R_g)/R_g \times 100$	40/329	155 °C	48

samples in ethanol is formed and printed on an alumina tube having length 4 mm and diameter 1,2 mm predeposited Au electrodes at the both end of tube. The 0.75% SWCNT Ag-$LaFeO_3$ showed good response even at low 1 ppm formaldehyde gas with very fast response and recovery times.

5. $LaFeO_3$ FOR OXIDIZING GASES SENSING

5.1. NO_2 Sensing. Sharma et al.[86] reported the preparation of $LaFeO_3$ and reduced graphene oxide (rGO)-$LaFeO_3$ microspheres by the hydrothermal method for the application for NO_2 sensor. They kept the solution at 160 °C for 6 h for fabrication of $LaFeO_3$ and then calcined it at 800 °C temperature. For the synthesis of rGO they adopted Hummer's method. The obtained samples were characterized and confirmed by XRD, FTIR, and XPS. The gas sensing device was fabricated by photolithography on an integrated electrode and IDE substrate with a size of 500 × 500 μm. The samples were tested with a device for gas sensing with a sourcing voltage of 6 V. This $LaFeO_3$ sensor shows a great response for 2 ppm NO_2 concentration with value of 144.1% at 250 °C. A sensor made by rGO-$LaFeO_3$ showed 183.4% response for 3 ppm NO_2 at a 250 °C operating temperature. Hence it is reported that rGO-$LaFeO_3$ exhibits a good response due to its higher surface area and smaller band gap with a bigger pore size.

Thirumalairajan et al.[87] reported the synthesis of $LaFeO_3$ thin films for the fabrication of a room temperature NO_2 sensor. They have two different morphologies for the sample prepared by radio frequency magnetron sputtering. The film thickness ranged from 100 to 800 nm under three wearing temperatures such as room temperature, 150 °C, and 300 °C. The morphology of obtained samples were nanocubes and a network structure. To study the gas sensing property, the films

https://doi.org/10.1021/acsomega.4c00334
ACS Omega 2024, 9, 29994−30014

Table 7. Carbon Dioxide (CO_2) Sensing Performance of $LaFeO_3$

material	method	doping	sensitivity	formula	time response/ recovery (s)	operating temp (°C)	ref
$La_{1-x}Sr_xFeO_3$	Sol−gel	Sr (X = 0.2)	1.25 @ 2000 ppm	R_g/R_a	11/5	380 °C	89
$LaFeO_3/SnO_2$	Sol−gel method	SnO_2 nano powder (La/Sn = 1:1)	2.72 (Sn-La) 1.72 @4000 ppm	R_a/R_g	20	250 °C. 275 °C	49
Polyaniline Mesoporous $LaFeO_3$	p−p Isotype heterojunctions	PANI (5−15%)	23.20 @20,000 ppm	$(R_a\text{-}R_g)/R_a \times 100$	90	27 °C	88

Table 8. Benzene Sensing Performance of Ag-$LaFeO_3$

material	method	doping	sensitivity	formula	operating temp (°C)	ref
Ag-$LaFeO_3$	Microwave chemical synthesis	B, Ag	17.5 1 ppm	R_g/R_a	65 °C	90

were sputtered onto a silicon substrate, and electric contacts were developed using copper wire and silver paste on the surface with an area 12 mm × 10 mm. The sensing value of network structure $LaFeO_3$ was 10.03−100.33 for 1−5 ppm NO_2 concentration. For the nanocube structures reported a higher response that is from 29.62 to 157.89 for 125 ppm NO_2 concentration, and response and recovery times were 24−11 s. and 35−15 s. respectively. It was also reported that a thin film has very good surface-active sites and good gas sensing performance for NO_2 as a test gas. Table 6 shows a summary of the NO_2 sensing results by $LaFeO_3$ based sensors.

$$NO_{2(ads)}^{-} + 2O_{2(ads)}^{-} \rightarrow 2O_{2(ads)}^{-} + NO_{2(g)} \quad (9)$$

5.2. Carbon Dioxide (CO_2) Sensing. Carbon dioxide (CO_2) is hazardous to human health and is a greenhouse gas that is produced due to the combustion of fossil fuels. So, the carbon dioxide detection and monitoring of its level have great importance today. Various metal oxides are used to develop CO_2 sensors, but $LaFeO_3$ shows very interesting results. Table 7 shows a summary of the CO_2 sensing results by $LaFeO_3$ based sensors.

Zhang et al.[49] reported the nanocomposite of $LaFeO_3$ with SnO_2 for the detection of CO_2. Initially $LaFeO_3$ was synthesized by the sol−gel method and combined with SnO_2. To fabricate the gas sensor a thick film of sample is deposited by the screen printing technique on a 36-matrices flat type material chip and annealed at 500 °C for 2 H. The sensors prepared by this composite exhibit a two times higher response than sensors fabricated by pure $LaFeO_3$ to CO_2 gas because the pn junction is formed between $LaFeO_3$ and SnO_2.

Hashemi Karouei et al.[88] developed mesoporous microspheres of $LaFeO_3$ with polymer for CO_2 sensing. This is a p-p type heterojunction, which shows excellent CO_2 sensing performance at room temperature. In this work different wt % values of $LaFeO_3$ with PANI were used for the CO_2 sensing, and it is observed that this p-p heterojunction showed a 13 times higher response than pure PANI gas sensors to CO_2 due to the decrease in the protonation state of PANI.

5.3. Benzene (C_6H_6) Sensing. A toxic compound benzene is produced due to burning of coal, gasoline, oil, and automobile exhaust. The toxic nature of benzene is mainly harmful to bone marrow and also enough to cause some other acute and chronic diseases like drowsiness, headaches, and aplastic etc. Benzene leak detection and monitoring have a main priority in the industrial area. The benzene sensing results are summarized in the Table 8.

Zhang et al.[90] developed a highly selective and sensitive heterojunction between boron-doped graphene quantum dots (BGQD) and a Ag-$LaFeO_3$ based benzene detector. Initially Ag-$LaFeO_3$ was molecularly imprinted by benzene, and then with the weight ratio 0.1%, 0.25%, 0.50%, 0.75%, and 1% of boron-doped graphene quantum dots was combined to form a p-p heterojunction. Figure 24 illustrates a possible benzene sensing mechanism. Due to the heterojunction with BGQD the carrier-transport ability of Ag-$LaFeO_3$ is improved, and hence the sensor works at the lower operating temperature compared to the pure $LaFeO_3$ based sensor.

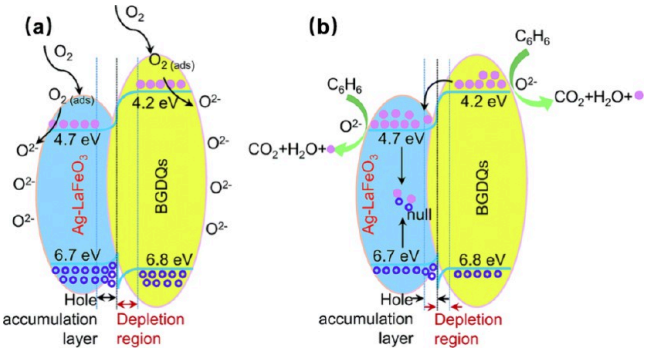

Figure 24. Gas sensing mechanism of boron-doped graphene quantum dots/Ag-$LaFeO_3$ (a) in air and (b) in benzene. Reprinted from ref 90. Copyright 2018, with permission from The Royal Society of Chemistry.

6. $LaFeO_3$ FOR A FEW OTHER GASES

The performance of $LaFeO_3$ for sensing some other important gases is reviewed and summarized in the Table 9.

7. STABILITY FOR $LaFeO_3$ BASED GAS SENSORS

Sensor's stability is also an important parameter which shows long-time stable functioning ability. Hence, for practical applications, long-term stability of the gas sensing material is the fundamental requirement. Many researchers studied the stability of the $LaFeO_3$ based sensors in their work. Experimental results obtained by the researchers during stability test are listed in Table 10. Most of the $LaFeO_3$ based gas sensors show a constant response for a long time, which indicates good stability of the material.

https://doi.org/10.1021/acsomega.4c00334
ACS Omega 2024, 9, 29994−30014

Table 9. Sensing Performance of $LaFeO_3$ toward Various Other Test Gases

material	method	doping	sensitivity	formula	time response/ recovery (s)	operating temp (°C)	ref
		Carbon Monoxide (CO)					
Crystalline cobalt/lead (Pb) codoped $LaFeO_3$	Modified Pechini route	$LaFe_{0.8}Co_{0.2}O_3$	91 @1660 ppm	$(R_g\text{-}R_a)/R_g \times 100$	95/75	175	50
$LaFeO_3$	Hydrothermal method	—	73 @200 ppm	$(R_g\text{-}R_a)/R_g \times 100$	20/4	240	54
$LaFeO_3$	Sol–gel citrate method	—	—	$(R_g\text{-}R_a)/R_g \times 100$	—	270	91
						350	
						420	
		Sulfur Dioxide (SO_2)					
		$SO_2 + O^- \rightarrow SO_3 + e^-$ (10)					
$LaFeO_3$	Soft polymerizable complex method	$La_{0.8}Ca_{0.2}FeO_2$ (20%)	50% ($La_{0.8}Ca_{0.2}$ $FeO_{2.95}$) 35% ($LaFeO_3$) @3 ppm	$(R_g\text{-}R_a)/R_g \times 100$	86/110	275	92
						180/280	
$La_{0.6}Ca_{0.4}FeO_3$ (thin films) $La_{1-x}Ca_xFeO_3$(pellets)	Sol–gel method	Ca ($0.4 \leq x \leq 0.8$	7.6	$(R_g\text{-}R_a)/R_g \times 100$	15/14	120	93
			3.6 @3 ppm @5 ppm		35/30	160	
		Trimethylamine $(CH_3)_3N$					
		$2(C_2H_5)_3N_{(gas)} + 39O^-_{(ads)} \leftrightarrow N_{2(ads)} + 12CO_{2(ads)} + 15H_2O_{(ads)} + 39e^-$ (11)					
rGO/$LaFeO_3$	Hydrothermal method (180 °C)	rGO (50:1 mg)	28.3 (pure)	R_g/R_a	–	260	94
			103.5 (rGO) @100 ppm			240	
RuO_2/$LaFeO_3$	Hydrothermal method	RuO_2	—	R_g/R_a	—	275	95
		Acetylene (C_2H_2)					
		$C_2H_2 + 5O^-_{(ads)} \rightarrow 3CO_2 + 3H_2O + 5e^-$ (12)					
Ag-loaded $LaFeO_3$	Flame spray pyrolysis	Ag (0.1 wt %)	60 @100 ppm	R_g/R_a	—	200	96
$LaFeO_3$	Sol–gel	—	500 ppm	R_g/R_a	—	150	97
		Tolene					
		$C_7H_{8(ads)} + 9O^-_2 \rightarrow 7CO_2 + 4H_2O + 9e^-$ (13)					
Ag-$LaFeO_3$	Molecular imprinted (sol–gel method assisted with microwave irradiation)	Ag (Ag: La = 1: 99)	24.0	R_g/R_a	90	215	98
			24.0 to @5 ppm				
		Xylene					
		$C_8H_{10(ads)} + 21O^- \rightarrow 8CO_{2(gas)} + 5H_2O_{(ads)} + 21e^-$ (14)					
Ag-$LaFeO_3$	Biotemplate via a sol–gel process molecular imprinting	Ag 91 mmol AgNO30	16.76 @10 ppm	R_g/R_a	68/36	125	99, 100
O_2							
$LaFeO_3$	Microwave-thermal treatment method, hydrothermal method, and sol–gel method	differed chemicals properties	O_2	R_g/R_a	42.7	450–1000	101, 102

https://doi.org/10.1021/acsomega.4c00334
ACS Omega 2024, 9, 29994−30014

Table 9. continued

material	method	doping	sensitivity	formula	time response/recovery (s)	operating temp (°C)	ref
		Ethylene (CH_3CH)					
$LaFeO_3$ thick-film	Coprecipitation	—	30 @0.2 ppm	R_g/R_a		250	103, 104
		Hydrogen (H_2)					
$LaFeO_3$	Sol–gel citrate	Sr x = 0.3 ($La_{1-x}Sr_xFeO_3$)	0.2 @500 ppm	$S = (R_a\text{-}R_g)/R_a$	20/270	325	42
$La_{1-x}Pb_xFeO_3$	Sol–gel at 60 °C	Pb (x = 0.2)	5 @ 500 ppm	R_g/R_a	10/40	160	78
$LaFeO_3$	Thermal decomposition of metal organic complex	Sr ($La_{0.3}Sr_{0.7}FeO_3$)	1.9 @ 30000 ppm	R_g/R_a	250	350	65

8. SUMMARY, CONCLUSION, AND FUTURE SCOPE

This review elucidates the gas-sensing capabilities of $LaFeO_3$ and the importance of gas sensors in environmental monitoring and their pivotal role in pollution control. The existing gas sensors available in the market and the research endeavors dedicated to advancing gas-sensor technology in past decade were evaluated. Furthermore, an assessment was conducted on a recent study about the potential use of $LaFeO_3$ in gas sensing applications. Additionally, a comprehensive list was provided, showcasing the oxidizing and reducing gases that $LaFeO_3$ can successfully detect. The study focuses on several synthesis methods for $LaFeO_3$ and the resulting changes in its morphologies. The reasons underlying its sensitivity to various gases and the detailed study findings on specific test gases were finally explained.

The future potential of $LaFeO_3$ based gas sensors is significant due to their crucial role in environmental monitoring and pollution management. As a result, there has been a substantial increase in the market demand for gas sensing devices. Metal oxides proved to be exceptional materials owing to their stability and sensitivity as gas sensors, which functions as both receptors and transducers. Notably, $LaFeO_3$ stands out as an efficient gas-sensing material due to its easy tunability of chemical compositions with partial substitution of other elements, and good thermal stability allows it to function at a wide temperature range and large number of active surface sites. As such, a total of 913 articles published in 2022 elaborated the gas-sensing behavior of $LaFeO_3$.

Among the various methods employed for its synthesis of $LaFeO_3$, the sol–gel and hydrothermal synthesis methods are reported most, while other methods gave different morphologies, as the electrospinning technique enables the production of $LaFeO_3$ in the form of nanobelts and nanowires. Furthermore, it was observed that hydrothermally grown $LaFeO_3$ heterostructures were patterned with α-Fe_2O_3 or $BaTiO_3$, yielding high responses for gases like acetone and ethanol, respectively. Also, the doping of silver enhances $LaFeO_3$'s gas-sensing abilities for the detection of methanol and formaldehyde gases. Further, the improved sensitivity of $LaFeO_3$ is reported to detect NO_2 and trimethylamine when combined with reduced graphene oxide (rGO). But some other gases like CO, SO_2, TEA, C_2H_5, C_6H_6, etc. can also be detected through a gas sensor based on $LaFeO_3$.

In fact, there are few limitations and challenges associated with using $LaFeO_3$ as a gas sensor. These are as follows:

- The requirement for high temperatures during the synthesis of $LaFeO_3$ can be a significant drawback, as it may limit the cost-effectiveness and practicality of large-scale production.
- Achieving nanoparticles of $LaFeO_3$ in the nanometer size range can be challenging. Nanoparticles are desirable for gas sensors because they offer a higher surface area, which enhances gas-surface interactions. Controlling the particle size precisely can be technically demanding.
- High resistivity can be a problem as it affects the gas sensing applications.
- The need for high operating temperatures can limit the practicality of $LaFeO_3$ gas sensors. High-temperature operation can lead to energy inefficiency.

https://doi.org/10.1021/acsomega.4c00334
ACS Omega 2024, 9, 29994−30014

Table 10. Stability of $LaFeO_3$ Based Gas Sensors

sr. no.	material and synthesis method	test gas	stability test	conclusion	ref
1	**$LaFeO_3$** radio frequency magnetron sputtering technique.	NO_2 (5 ppm)	60 days with interval of 10 days	Slight increase in the resistance baseline with good sensing stability	87
2	**$La_{1-x}Sr_xFeO_3$** sol−gel citrate	Acetone (500 ppm)	60 days with interval of 10 days	Constant response with good stability	42
3	**Ag-$LaFeO_3$** molecular imprinted (sol−gel method assisted with microwave irradiation)	Toluene (5 ppm)	15 days	Excellent long-time stability	98
4	**$LaFeO_3$** biotemplate via a sol−gel process molecular imprinting	Xylene (10 ppm)	30 days with interval of 2 days	No significant change in the sensor response which confirms excellent stability	99
5	**BGQD/Ag-$LaFeO_3$** Microwave chemical synthesis.	Benzene (1 ppm)	40 days	Good stability	90
6	**$LaFe_{1-x}Mn_xO_3$** Sol−gel method	Ethanol (50 ppm)	40 days with interval of 5 days	Response of sensor is decreased by 7.8%	79
7	**$LaFeO_3$microspheres** Hydrothermal	Acetone (50 ppm)	60 days with interval of 10 days	No significant change in the sensor response which confirms excellent stability	43
8	**$LaFeO_3$ yolk shell** Hydrothermal method (annealing and etching)	Acetone (100 ppm)	30 days with interval of 1 days	Good relative stability	44
9	**$BaTiO_3/LaFeO_3$** Citric sol−gel method	Ethanol	96 h	Good stability	32
10	**$La_{1-x}Pb_xFeO_3$** Sol−gel at 60 °C	Ethanol (500 ppm)	100 h	Stable response	78

- $LaFeO_3$ exhibits a slow response and recovery when exposed to gases, which can be a limitation in applications where rapid detection and measurement of gas concentrations are essential

In addition to the aforementioned limitations, there are practical challenges that need to be addressed to make it more suitable for commercial use.

In conclusion, the trends in the research on $LaFeO_3$ perovskite elucidate the following opportunities and Scope:

- The gas sensing behavior of a material depends significantly on its surface morphology and structural characteristics. $LaFeO_3$ offers opportunities for modifying its structure and morphology during synthesis by adjusting parameters such as temperature, reaction time, and synthesis techniques. These modifications can have a significant impact on its gas-sensing properties.
- Creating heterostructures by combining $LaFeO_3$ with n-type metal-oxide semiconductors (MOSs) can be beneficial for improving the sensing properties of $LaFeO_3$. This approach involves integrating different materials to create a composite structure that may have synergistic effects on gas sensing.
- Doping $LaFeO_3$ with materials like reduced graphene oxide (rGO) or silver (Ag), palladium (Pd), and other suitable elements in specific quantities offers the potential to develop ultrahigh-sensitive materials for detecting toxic and combustible gases. Doping involves introducing small amounts of other elements into the material to modify its electronic properties and enhance its gas-sensing capabilities.
- The incorporation of different surfactants into $LaFeO_3$ can increase the surface-to-volume ratio, roughness, and porosity of the material. These changes can enhance the surface adsorption mechanism, making it more effective at detecting and interacting with gases.

AUTHOR INFORMATION

Corresponding Authors

Digambar Y. Nadargi − *Centre for Materials for Electronics Technology, CMET, Thrissur 680581, India;* orcid.org/0000-0003-2092-2590; Email: digambar_nadargi@yahoo.co.in

Nguyen Tam Nguyen Truong − *School of Chemical Engineering, Yeungnam University, Gyeongsan 38541, Korea;* Email: tamnguyentn@ynu.ac.kr

Sharad S. Suryavanshi − *School of Physical Sciences, PAH Solapur University, Solapur 413255, India;* orcid.org/0000-0002-3996-1998; Email: sssuryavanshi@rediffmail.com

Authors

Suraj S. Patil − *School of Physical Sciences, PAH Solapur University, Solapur 413255, India; Department of Physics, Yashavantrao Chavan Institute of Science, Satara 415001, India*

Bapuso M. Babar − *Department of Physics, Yashavantrao Chavan Institute of Science, Satara 415001, India*

Faiyyaj I. Shaikh − *Department of Forensic Physics, Government Institute of Forensic Science, Aurangabad 431004, India*

Jyoti D. Nadargi − *Department of Physics, Santosh Bhimrao Patil College, Mandrup, Solapur 413221, India*

Babasaheb R. Sankapal − *Department of Physics, Visvesvaraya National Institute of Technology, Nagpur 440010, India*

Imtiaz S. Mulla − *Former Emeritus Scientist, NCL, Pune 411008, India*

Mohaseen S. Tamboli − *Korea Institute of Energy Technology (KENTECH), Naju, Jeollanam-do 58330, Republic of Korea*

Complete contact information is available at: https://pubs.acs.org/10.1021/acsomega.4c00334

Notes

The authors declare no competing financial interest.

ACKNOWLEDGMENTS

The authors acknowledge the Yashavantrao Chavan Institute of Science, Satara for financial support of this work through Project No. RSS/YCIS/2020-21/RDC/RUSA-4 received by Suraj S. Patil.

https://doi.org/10.1021/acsomega.4c00334
ACS Omega 2024, 9, 29994−30014

REFERENCES

(1) Majhi, S. M.; Mirzaei, A.; Kim, H. W.; Kim, S. S.; Kim, T. W. Recent Advances in Energy-Saving Chemi-resistive Gas Sensors: A Review. *Nano Energy* **2021**, *79*, 105369.

(2) Glencross, D. A.; Ho, T. R.; Camiña, N.; Hawrylowicz, C. M.; Pfeffer, P. E. Air Pollution and Its Effects on the Immune System. *Free Radical Biol. Med.* **2020**, *151*, 56−68, DOI: 10.1016/j.freeradbiomed.2020.01.179.

(3) Shetty, S. S.; D, D.; S, H.; Sonkusare, S.; Naik, P. B.; Kumari, N. S.; Madhyastha, H. Environmental Pollutants and Their Effects on Human Health. *Heliyon* **2023**, *9*, E19496 DOI: 10.1016/j.heliyon.2023.e19496.

(4) Schraufnagel, D. E.; Balmes, J. R.; Cowl, C. T.; De Matteis, S.; Jung, S. H.; Mortimer, K.; Perez-Padilla, R.; Rice, M. B.; Riojas-Rodriguez, H.; Sood, A.; Thurston, G. D.; To, T.; Vanker, A.; Wuebbles, D. J. Air Pollution and Noncommunicable Diseases: A Review by the Forum of International Respiratory Societies' Environmental Committee, Part 2: Air Pollution and Organ Systems. *Chest* **2019**, *155*, 417−426, DOI: 10.1016/j.chest.2018.10.041.

(5) Com, I. *Air Pollution and Child Health*; 2018. http://apps.who.int/bookorders.

(6) Kaur, R.; Pandey, P. Air Pollution, Climate Change, and Human Health in Indian Cities: A Brief Review. *Frontiers in Sustainable Cities* **2021**, *3*. DOI: 10.3389/frsc.2021.705131.

(7) Tiotiu, A. I.; Novakova, P.; Nedeva, D.; Chong-Neto, H. J.; Novakova, S.; Steiropoulos, P.; Kowal, K. Impact of Air Pollution on Asthma Outcomes. *International Journal of Environmental Research and Public Health* **2020**, *17*, 6212−29, DOI: 10.3390/ijerph17176212.

(8) Popov, O.; Iatsyshyn, A.; Kovach, V.; Artemchuk, V.; Kameneva, I.; Taraduda, D.; Sobyna, V.; Sokolov, D.; Dement, M.; Yatsyshyn, T. Risk Assessment for the Population of Kyiv, Ukraine as a Result of Atmospheric Air Pollution. *J. Health Pollut* **2020**, *10* (25). DOI: 10.5696/2156-9614-10.25.200303.

(9) Zhang, H.; Zhang, D.; Zhang, B.; Wang, D.; Tang, M. Wearable Pressure Sensor Array with Layer-by-Layer Assembled MXene Nanosheets/Ag Nanoflowers for Motion Monitoring and Human-Machine Interfaces. *ACS Appl. Mater. Interfaces* **2022**, *14* (43), 48907−48916.

(10) Zhang, H.; Chen, X.; Liu, Y.; Yang, C.; Liu, W.; Qi, M.; Zhang, D. PDMS Film-Based Flexible Pressure Sensor Array with Surface Protruding Structure for Human Motion Detection and Wrist Posture Recognition. *ACS Appl. Mater. Interfaces* **2024**, *16* (2), 2554−2563.

(11) Chen, Q.; Zhang, Y.; Tang, M.; Wang, Z.; Zhang, D. A Fast Response Hydrogen Sensor Based on the Heterojunction of MXene and SnO_2 Nanosheets for Lithium-Ion Battery Failure Detection. *Sens Actuators B Chem.* **2024**, *405*, 135229.

(12) Feng, S.; Farha, F.; Li, Q.; Wan, Y.; Xu, Y.; Zhang, T.; Ning, H. Review on Smart Gas Sensing Technology. *Sensors (Switzerland)* **2019**, *19*, 3760 DOI: 10.3390/s19173760.

(13) Zhang, D.; Sun, Y.; Li, P.; Zhang, Y. Facile Fabrication of MoS_2-Modified SnO_2 Hybrid Nanocomposite for Ultrasensitive Humidity Sensing. *ACS Appl. Mater. Interfaces* **2016**, *8* (22), 14142−14149.

(14) Gas Sensors- A Review. *Journal of Environmental Nanotechnology* **2015**, *4* (4), 01−14. .

(15) Gautam, Y. K.; Sharma, K.; Tyagi, S.; Ambedkar, A. K.; Chaudhary, M.; Pal Singh, B. Nanostructured Metal Oxide Semiconductor-Based Sensors for Greenhouse Gas Detection: Progress and Challenges. *Royal Society Open Science* **2021**, *8*. DOI: 10.1098/rsos.201324.

(16) Zhang, D.; Mi, Q.; Wang, D.; Li, T. MXene/Co_3O_4 Composite Based Formaldehyde Sensor Driven by ZnO/MXene Nanowire Arrays Piezoelectric Nanogenerator. *Sens Actuators B Chem.* **2021**, *339*, 129923.

(17) Kang, Z.; Zhang, D.; Li, T.; Liu, X.; Song, X. Polydopamine-Modified SnO_2 Nanofiber Composite Coated QCM Gas Sensor for High-Performance Formaldehyde Sensing. *Sens Actuators B Chem.* **2021**, *345*, 130299.

(18) Babar, B. M.; Sutar, S. H.; Mujawar, S. H.; Patil, S. S.; Babar, U. D.; Pawar, U. T.; Kadam, P. M.; Patil, P. S.; Kadam, L. D. V_2O_5-RGO Based Chemiresistive Gas Sensor for NO_2 Detection. *Materials Science and Engineering: B* **2023**, *298*, 116827.

(19) Myadam, N. L.; Nadargi, D. Y.; Gurav Nadargi, J. D.; Shaikh, F. I.; Suryavanshi, S. S.; Chaskar, M. G. A Facile Approach of Developing Al/SnO_2 Xerogels via Epoxide Assisted Gelation: A Highly Versatile Route for Formaldehyde Gas Sensors. *Inorg. Chem. Commun.* **2020**, *116*, 107901.

(20) Nadargi, D. Y.; Dateer, R. B.; Tamboli, M. S.; Mulla, I. S.; Suryavanshi, S. S. A Greener Approach towards the Development of Graphene-Ag Loaded ZnO Nanocomposites for Acetone Sensing Applications. *RSC Adv.* **2019**, *9* (58), 33602−33606.

(21) Sonawane, N. B.; Baviskar, P. K.; Ahire, R. R.; Sankapal, B. R. CdO Necklace like Nanobeads Decorated with PbS Nanoparticles: Room Temperature LPG Sensor. *Mater. Chem. Phys.* **2017**, *191*, 168−172.

(22) Sonawane, N. B.; Gurav, K. V.; Ahire, R. R.; Kim, J. H.; Sankapal, B. R. CdS Nanowires with PbS Nanoparticles Surface Coating as Room Temperature Liquefied Petroleum Gas Sensor. *Sens Actuators A Phys.* **2014**, *216*, 78−83.

(23) Ladhe, R. D.; Gurav, K. V.; Pawar, S. M.; Kim, J. H.; Sankapal, B. R. P-PEDOT:PSS as a Heterojunction Partner with n-ZnO for Detection of LPG at Room Temperature. *J. Alloys Compd.* **2012**, *515*, 80−85.

(24) Ladhe, R. D.; Baviskar, P. K.; Tan, W. W.; Zhang, J. B.; Lokhande, C. D.; Sankapal, B. R. LPG Sensor Based on Complete Inorganic N-Bi_2S_3-P-CuSCN Heterojunction Synthesized by a Simple Chemical Route. *J. Phys. D Appl. Phys.* **2010**, *43* (24), 245302.

(25) Mehta, S. S.; Tamboli, M. S.; Mulla, I. S.; Suryavanshi, S. S. CTAB Assisted Synthesis of Tungsten Oxide Nanoplates as an Efficient Low Temperature NO_X Sensor. *J. Solid State Chem.* **2018**, *258*, 256−263.

(26) Tang, M.; Zhang, D.; Sun, Y.; Wang, Z.; Xi, G.; Chen, Q.; Mao, R.; Zhang, H. Chemiresistive Detection of SO_2 in SF_6 Decomposition Products Based on ZnO Nanorod/MoS_2 Nanoflower Heterojunctions: Experimental and First-Principles Investigations. *Sens Actuators B Chem.* **2024**, *403*, 135170.

(27) Zhou, D.; Kang, Z.; Liu, X.; Yan, W.; Cai, H.; Xu, J.; Zhang, D. High Sensitivity Ammonia QCM Sensor Based on ZnO Nanoflower Assisted Cellulose Acetate-Polyaniline Composite Nanofibers. *Sens Actuators B Chem.* **2023**, *392*, 134072.

(28) Tang, M.; Zhang, D.; Chen, Q.; Wang, Z.; Wang, D.; Yang, Z.; Xu, W.; Wang, L.; Zhu, L.; An, F. Heterostructure Construction of SnS_2 Debye Nanowires Modified with ZnO Nanorods for Chemiresistive H_2S Detection in Sulfur Hexafluoride Decomposition Products. *Sens Actuators B Chem.* **2023**, *390*, 133952.

(29) Rong, Q.; Zhang, Y.; Li, K.; Wang, H.; Hu, J.; Zhu, Z.; Zhang, J.; Liu, Q. Ag-$LaFeO_3$ /NCQDs p-n Heterojunctions for Superior Methanol Gas Sensing Performance. *Mater. Res. Bull.* **2019**, *115*, 55−64.

(30) Yin, X. T.; Dastan, D.; Wu, F. Y.; Li, J. Facile Synthesis of SnO_2/$LaFeO_{3-x}$ N_x Composite: Photocatalytic Activity and Gas Sensing Performance. *Nanomaterials* **2019**, *9* (8), 1163.

(31) Khan, I.; Sun, N.; Wang, Y.; Li, Z.; Qu, Y.; Jing, L. Synthesis of SnO_2/Yolk-Shell $LaFeO_3$ Nanocomposites as Efficient Visible-Light Photocatalysts for 2,4-Dichlorophenol Degradation. *Mater. Res. Bull.* **2020**, *127*, 110857.

(32) Wang, H.; Guo, Z.; Hao, W.; Sun, L.; Zhang, Y.; Cao, E. Ethanol Sensing Characteristics of $BaTiO_3$/$LaFeO_3$ Nanocomposite. *Mater. Lett.* **2019**, *234*, 40−44.

(33) Fan, H.; Zhang, T.; Xu, X.; Lv, N. Fabrication of N-Type Fe_2O_3 and P-Type $LaFeO_3$ Nanobelts by Electrospinning and Determination of Gas-Sensing Properties. *Sens Actuators B Chem.* **2011**, *153* (1), 83−88.

(34) Zhang, D.; Chen, M.; Zou, H.; Zhang, Y.; Hu, J.; Wang, H.; Zi, B.; Zhang, J.; Zhu, Z.; Duan, L.; Liu, Q. Microwave-Assisted Synthesis of Porous and Hollow α-Fe_2O_3/$LaFeO_3$ Nanostructures for Acetone

https://doi.org/10.1021/acsomega.4c00334
ACS Omega 2024, 9, 29994−30014

Gas Sensing as Well as Photocatalytic Degradation of Methylene Blue. *Nanotechnology* **2020**, *31* (21), 215601.
(35) Kubacka, A.; Fernández-García, M.; Colón, G. Advanced Nanoarchitectures for Solar Photocatalytic Applications. *Chem. Rev.* **2012**, *112*, 1555−1614.
(36) Thuy, N. T.; Cong, B. T.; Minh, D. Le. The Structural and Magnetic Properties of the Double Rearth Elements La_{1-x} Nd_x FeO_3 Nanoparticles. *ISRN Materials Science* **2012**, *2012*, 1−6.
(37) Rai, A.; Sharma, A. L.; Thakur, A. K. Evaluation of Aluminium Doped Lanthanum Ferrite Based Electrodes for Supercapacitor Design. *Solid State Ion* **2014**, *262*, 230−233.
(38) John Berchmans, L.; Sindhu, R.; Angappan, S.; Augustin, C. O. Effect of Antimony Substitution on Structural and Electrical Properties of $LaFeO_3$. *J. Mater. Process Technol.* **2008**, *207* (1−3), 301−306.
(39) Pirzada, B. M.; Pushpendra; Kunchala, R. K.; Naidu, B. S. Synthesis of $LaFeO_3/Ag_2CO_3$ Nanocomposites for Photocatalytic Degradation of Rhodamine B and p-Chlorophenol under Natural Sunlight. *ACS Omega* **2019**, *4* (2), 2618−2629.
(40) Yang, K.; Ma, J.; Qiao, X.; Cui, Y.; Jia, L.; Wang, H. Hierarchical Porous $LaFeO_3$ Nanostructure for Efficient Trace Detection of Formaldehyde. *Sens Actuators B Chem.* **2020**, *313*, 128022.
(41) Ji, H.; Zeng, W.; Li, Y. Gas Sensing Mechanisms of Metal Oxide Semiconductors: A Focus Review. *Nanoscale* **2019**, *11*, 22664−22684, DOI: 10.1039/c9nr07699a.
(42) Murade, P. A.; Sangawar, V. S.; Chaudhari, G. N.; Kapse, V. D.; Bajpeyee, A. U. Acetone Gas-Sensing Performance of Sr-Doped Nanostructured $LaFeO_3$ Semiconductor Prepared by Citrate Sol-Gel Route. *Curr. Appl. Phys.* **2011**, *11* (3), 451−456.
(43) Xiao, H.; Xue, C.; Song, P.; Li, J.; Wang, Q. Preparation of Porous $LaFeO_3$ Microspheres and Their Gas-Sensing Property. *Appl. Surf. Sci.* **2015**, *337*, 65−71.
(44) Wang, B.; Yu, Q.; Zhang, S.; Wang, T.; Sun, P.; Chuai, X.; Lu, G. Gas Sensing with Yolk-Shell $LaFeO_3$ Microspheres Prepared by Facile Hydrothermal Synthesis. *Sens Actuators B Chem.* **2018**, *258*, 1215−1222.
(45) Zhang, H.; Song, P.; Han, D.; Wang, Q. Synthesis and Formaldehyde Sensing Performance of $LaFeO_3$ Hollow Nanospheres. *Physica E Low Dimens Syst. Nanostruct* **2014**, *63*, 21−26.
(46) Wei, W.; Guo, S.; Chen, C.; Sun, L.; Chen, Y.; Guo, W.; Ruan, S. High Sensitive and Fast Formaldehyde Gas Sensor Based on Ag-Doped $LaFeO_3$ nanofibers. *J. Alloys Compd.* **2017**, *695*, 1122−1127.
(47) Rong, Q.; Zhang, Y.; Lv, T.; Shen, K.; Zi, B.; Zhu, Z.; Zhang, J.; Liu, Q. Highly Selective and Sensitive Methanol Gas Sensor Based on Molecular Imprinted Silver-Doped $LaFeO_3$ Core-Shell and Cage Structures. *Nanotechnology* **2018**, *29* (14), 145503.
(48) Zhang, X. D.; Zhang, W. L.; Cai, Z. X.; Li, Y. K.; Yamauchi, Y.; Guo, X. $LaFeO_3$ Porous Hollow Micro-Spindles for NO_2 Sensing. *Ceram. Int.* **2019**, *45* (5), 5240−5248.
(49) Zhang, W.; Xie, C.; Zhang, G.; Zhang, J.; Zhang, S.; Zeng, D. Porous $LaFeO_3/SnO_2$ Nanocomposite Film for CO_2 Detection with High Sensitivity. *Mater. Chem. Phys.* **2017**, *186*, 228−236.
(50) Bhargav, K. K.; Ram, S.; Labhsetwar, N.; Majumder, S. B. Correlation of Carbon Monoxide Sensing and Catalytic Activity of Pure and Cation Doped Lanthanum Iron Oxide Nano-Crystals. *Sens Actuators B Chem.* **2015**, *206*, 389−398.
(51) Feng, J.; Liu, T.; Xu, Y.; Zhao, J.; He, Y. Effects of PVA Content on the Synthesis of $LaFeO_3$ via Sol-Gel Route. *Ceram. Int.* **2011**, *37* (4), 1203−1207.
(52) Farhadi, S.; Momeni, Z.; Taherimehr, M. Rapid Synthesis of Perovskite-Type $LaFeO_3$ Nanoparticles by Microwave-Assisted Decomposition of Bimetallic $La[Fe(CN)_6]\cdot 5H_2O$ Compound. *J. Alloys Compd.* **2009**, *471*, L5.
(53) Thirumalairajan, S.; Girija, K.; Ganesh, I.; Mangalaraj, D.; Viswanathan, C.; Balamurugan, A.; Ponpandian, N. Controlled Synthesis of Perovskite $LaFeO_3$ Microsphere Composed of Nanoparticles via Self-Assembly Process and Their Associated Photocatalytic Activity. *Chemical Engineering Journal* **2012**, *209*, 420−428.
(54) Song, P.; Wang, Q. Hydrothermal Synthesis and Gas Sensing Properties of $LaFeO_3$*Proceedings of the 7th National Conference on Functional Materials and Applications*; FMA, 2010.
(55) Phan, T. T. N.; Nikoloski, A. N.; Bahri, P. A.; Li, D. Optimizing Photocatalytic Performance of Hydrothermally Synthesized $LaFeO_3$ by Tuning Material Properties and Operating Conditions. *J. Environ. Chem. Eng.* **2018**, *6* (1), 1209−1218.
(56) Mesbah, M.; Hamedshahraki, S.; Ahmadi, S.; Sharifi, M.; Igwegbe, C. A. Hydrothermal synthesis of LaFeO3 nanoparticles adsorbent: Characterization and application of error functions for adsorption of fluoride. *MethodsX* **2020**, *7*, 100786−100801.
(57) Kostyukhin, E. M.; Kustov, A. L.; Kustov, L. M. One-Step Hydrothermal Microwave-Assisted Synthesis of $LaFeO_3$ Nanoparticles. *Ceram. Int.* **2019**, *45* (11), 14384−14388.
(58) Dhinesh Kumar, R.; Jayavel, R. Facile Hydrothermal Synthesis and Characterization of $LaFeO_3$ Nanospheres for Visible Light Photocatalytic Applications. *Journal of Materials Science: Materials in Electronics* **2014**, *25* (9), 3953−3961.
(59) Hao, P.; Lin, Z.; Song, P.; Yang, Z.; Wang, Q. Hydrothermal Preparation and Acetone-Sensing Properties of Ni-Doped Porous $LaFeO_3$ Microspheres. *Journal of Materials Science: Materials in Electronics* **2020**, *31* (9), 6679−6689.
(60) Nikam, S. K.; Athawale, A. A. Phase Formation Study of Noble Metal (Au, Ag and Pd) Doped Lanthanum Perovskites Synthesized by Hydrothermal Method. *Mater. Chem. Phys.* **2015**, *155*, 104−112.
(61) Deng, J.; Dai, H.; Jiang, H.; Zhang, L.; Wang, G.; He, H.; Chak Tong, A. U. Hydrothermal Fabrication and Catalytic Properties of La_{1-X} Sr_x M_{1-Y} Fe_y O_3 (M = Mn, Co) That Are Highly Active for the Removal of Toluene. *Environ. Sci. Technol.* **2010**, *44* (7), 2618−2623.
(62) Li, F.-T.; Liu, S.-J.; Xue, Y.-B.; Wang, X.-J.; Hao, Y.-J.; Zhao, J.; Liu, R.-H.; Zhao, D. Structure Modification Function of g-C_3N_4 for Al_2O_3 in the In Situ Hydrothermal Process for Enhanced Photocatalytic Activity. *Chem. Eur. J.* **2015**, *21*, 10149−10159.
(63) Rong, Q.; Zhang, Y.; Hu, J.; Li, K.; Wang, H.; Chen, M.; Lv, T.; Zhu, Z.; Zhang, J.; Liu, Q. Design of Ultrasensitive Ag-$LaFeO_3$ Methanol Gas Sensor Based on Quasi Molecular Imprinting Technology. *Sci. Rep.* **2018**, *8* (1). DOI: 10.1038/s41598-018-32113-x.
(64) Qin, J.; Cui, Z.; Yang, X.; Zhu, S.; Li, Z.; Liang, Y. Synthesis of Three-Dimensionally Ordered Macroporous $LaFeO_3$ with Enhanced Methanol Gas Sensing Properties. *Sens Actuators B Chem.* **2015**, *209*, 706−713.
(65) Koonsaeng, N.; Thaweechai, T.; Wisitsoraat, A.; Wattanathana, W.; Wannapaiboon, S.; Chotiwan, S.; Veranitisagul, C.; Laobuthee, A. *Preparation of Sr-Doped $LaFeO_3$ by Thermal Decomposition of Metal Organic Complex and Their Gas-Sensing Properties*, 2018. www.symbiosisonline.orgwww.symbiosisonlinepublishing.com.
(66) Matei, C.; Berger, D.; Stoleriu, S.; Papa, F.; Fruth, V. Synthesis of Lanthanum Ferrite Nanopowder by Combustion Method. *Optoelectronics Adv. Mater.-Rapid Commun.* **2007**, *9*, 1793.
(67) Bellakki, M. B.; Manivannan, V. Solution Combustion Synthesis of (La, K) FeO3 Orthoferrite Ceramics: Structural and Magnetic Property Studies. *Bull. Mater. Sci.* **2010**, *33*, 611.
(68) Bellakki, M. B.; Kelly, B. J.; Manivannan, V. Synthesis, Characterization, and Property Studies of (La, Ag) FeO_3 ($0.0 \leq x \leq 0.3$) Perovskites. *J. Alloys Compd.* **2010**, *489* (1), 64−71.
(69) Lee, W. Y.; Yun, H. J.; Yoon, J. W. Characterization and Magnetic Properties of $LaFeO_3$ Nanofibers Synthesized by Electrospinning. *J. Alloys Compd.* **2014**, *583*, 320−324.
(70) Shi, X.; Zhou, W.; Ma, D.; Ma, Q.; Bridges, D.; Ma, Y.; Hu, A. Electrospinning of Nanofibers and Their Applications for Energy Devices. *J. Nanomater.* **2015**. DOI: 10.1155/2015/140716.
(71) Leng, J.; Li, S.; Wang, Z.; Xue, Y.; Xu, D. Synthesis of Ultrafine Lanthanum Ferrite ($LaFeO_3$) Fibers via Electrospinning. *Mater. Lett.* **2010**, *64* (17), 1912−1914.
(72) Xie, Y.; Kocaefe, D.; Chen, C.; Kocaefe, Y. Review of Research on Template Methods in Preparation of Nanomaterials. *J. Nanomater.* **2016**. DOI: 10.1155/2016/2302595.

https://doi.org/10.1021/acsomega.4c00334
ACS Omega 2024, 9, 29994−30014

(73) Zhang, Q.; Wang, W.; Goebl, J.; Yin, Y. Self-Templated Synthesis of Hollow Nanostructures. *Nano Today.* **2009**, *4*, 494−507.
(74) Majedi, A.; Abbasi, A.; Davar, F. Green Synthesis of Zirconia Nanoparticles Using the Modified Pechini Method and Characterization of Its Optical and Electrical Properties. *J. Solgel Sci. Technol.* **2016**, *77* (3), 542−552.
(75) Rezaei, M.; Mirkazemi, S. M.; Alamolhoda, S. The Role of PVA Surfactant on Magnetic Properties of $MnFe_2O_4$ Nanoparticles Synthesized by Sol-Gel Hydrothermal Method. *J. Supercond Nov Magn* **2021**, *34* (5), 1397−1408.
(76) Chen, Y.; Qin, H.; Wang, X.; Li, L.; Hu, J. Acetone Sensing Properties and Mechanism of Nano-$LaFeO_3$ Thick-Films. *Sens Actuators B Chem.* **2016**, *235*, 56−66.
(77) Song, P.; Zhang, H.; Han, D.; Li, J.; Yang, Z.; Wang, Q. Preparation of Biomorphic Porous $LaFeO_3$ by Sorghum Straw Biotemplate Method and Its Acetone Sensing Properties. *Sens Actuators B Chem.* **2014**, *196*, 140−146.
(78) Song, P.; Qin, H.; Zhang, L.; An, K.; Lin, Z.; Hu, J.; Jiang, M. The Structure, Electrical and Ethanol-Sensing Properties of $La_{1-X}Pb_xFeO_3$ Perovskite Ceramics with $x \leq 0.3$. *Sens Actuators B Chem.* **2005**, *104* (2), 312−316.
(79) Li, F.; Wang, Z.; Wang, A.; Wu, S.; Zhang, L. N-Type $LaFe_{1-X}Mn_xO_3$ Prepared by Sol-Gel Method for Gas Sensing. *J. Alloys Compd.* **2020**, *816*, 152647.
(80) Cao, K.; Cao, E.; Zhang, Y.; Hao, W.; Sun, L.; Peng, H. The Influence of Nonstoichiometry on Electrical Transport and Ethanol Sensing Characteristics for Nanocrystalline $LaFeO_3$- Sensors. *Sens Actuators B Chem.* **2016**, *230*, 592−599.
(81) Fan, K.; Qin, H.; Zhang, Z.; Sun, L.; Sun, L.; Hu, J. Gas Sensing Properties of Nanocrystalline La 0.75Ba 0.25FeO_3Thick-Film Sensors. *Sens Actuators B Chem.* **2012**, *171*−*172*, 302−308.
(82) Rong, Q.et al. Excellent Methanol Sensing Performance of Gas Sensor Based on Ag-$LaFeO_3$ Modified with Graphene. *J. Mol. Sci.* **2018**, *2*. https://www.imedpub.com/articles-pdfs/excellent-methanol-sensing-performance-of-gas-sensor-based-on-aglafeo3-modified-with-graphene.pdf.
(83) Rong, Q.; Zhang, Y.; Wang, C.; Zhu, Z.; Zhang, J.; Liu, Q. A High Selective Methanol Gas Sensor Based on Molecular Imprinted Ag-$LaFeO_3$ Fibers. *Sci. Rep.* **2017**, *7* (1). DOI: 10.1038/s41598-017-12337-z.
(84) Zhang, Y. M.; Zhang, J.; Chen, J. L.; Zhu, Z. Q.; Liu, Q. J. Improvement of Response to Formaldehyde at Ag-$LaFeO_3$ Based Gas Sensors through Incorporation of SWCNTs. *Sens Actuators B Chem.* **2014**, *195*, 509−514.
(85) Zhang, Y.; Zhao, J.; Sun, H.; Zhu, Z.; Zhang, J.; Liu, Q. B, N, S, Cl Doped Graphene Quantum Dots and Their Effects on Gas-Sensing Properties of Ag-$LaFeO_3$. *Sens Actuators B Chem.* **2018**, *266*, 364−374.
(86) Sharma, N.; Kushwaha, H. S.; Sharma, S. K.; Sachdev, K. Fabrication of $LaFeO_3$ and RGO-$LaFeO_3$ Microspheres Based Gas Sensors for Detection of NO_2 and CO. *RSC Adv.* **2020**, *10* (3), 1297−1308.
(87) Thirumalairajan, S.; Girija, K.; Mastelaro, V. R.; Ponpandian, N. Surface Morphology-Dependent Room-Temperature $LaFeO_3$ Nanostructure Thin Films as Selective NO_2 Gas Sensor Prepared by Radio Frequency Magnetron Sputtering. *ACS Appl. Mater. Interfaces* **2014**, *6* (16), 13917−13927.
(88) Hashemi Karouei, S. F.; Milani Moghaddam, H. P-p Heterojunction of Polymer/Hierarchical Mesoporous $LaFeO_3$ Microsphere as CO_2 Gas Sensing under High Humidity. *Appl. Surf. Sci.* **2019**, *479*, 1029−1038.
(89) Fan, K.; Qin, H.; Wang, L.; Ju, L.; Hu, J. CO_2 Gas Sensors Based on $La_{1-X}Sr_xFeO_3$ Nanocrystalline Powders. *Sens Actuators B Chem.* **2013**, *177*, 265−269.
(90) Zhang, Y.; Rong, Q.; Zhao, J.; Zhang, J.; Zhu, Z.; Liu, Q. Boron-Doped Graphene Quantum Dot/Ag-$LaFeO_3$ p-p Heterojunctions for Sensitive and Selective Benzene Detection. *J. Mater. Chem. A Mater.* **2018**, *6* (26), 12647−12653.
(91) Toan, N. N.; Saukko, S.; Lantto, V. Gas Sensing with Semiconducting Perovskite Oxide $LaFeO_3$. *Physica B: Condensed Matter* **2003**, *327*, 279.
(92) Palimar, S.; Kaushik, S. D.; Siruguri, V.; Swain, D.; Viegas, A. E.; Narayana, C.; Sundaram, N. G. Investigation of Ca Substitution on the Gas Sensing Potential of LaFeO3 Nanoparticles towards Low Concentration SO_2 Gas. *Dalton Transactions* **2016**, *45* (34), 13547−13555.
(93) Aranthady, C.; Jangid, T.; Gupta, K.; Mishra, A. K.; Kaushik, S. D.; Siruguri, V.; Rao, G. M.; Shanbhag, G. V.; Sundaram, N. G. Selective SO_2 Detection at Low Concentration by Ca Substituted $LaFeO_3$ Chemiresistive Gas Sensor: A Comparative Study of $LaFeO_3$ Pellet vs Thin Film. *Sens Actuators B Chem.* **2021**, *329*, 129211.
(94) Hao, P.; Lin, Z.; Song, P.; Yang, Z.; Wang, Q. RGO-Wrapped Porous $LaFeO_3$ Microspheres for High-Performance Triethylamine Gas Sensors. *Ceram. Int.* **2020**, *46* (7), 9363−9369.
(95) Hao, P.; Song, P.; Yang, Z.; Wang, Q. Synthesis of Novel RuO_2/$LaFeO_3$ Porous Microspheres Its Gas Sensing Performances towards Triethylamine. *J. Alloys Compd.* **2019**, *806*, 960−967.
(96) Sukee, A.; Alharbi, A. A.; Staerz, A.; Wisitsoraat, A.; Liewhiran, C.; Weimar, U.; Barsan, N. Effect of AgO Loading on Flame-Made $LaFeO_3$ p-Type Semiconductor Nanoparticles to Acetylene Sensing. *Sens Actuators B Chem.* **2020**, *312*, 127990.
(97) Alharbi, A. A.; Sackmann, A.; Weimar, U.; Bârsan, N. Acetylene- And Ethylene-Sensing Mechanism for $LaFeO_3$-Based Gas Sensors: Operando Insights. *J. Phys. Chem. C* **2020**, *124* (13), 7317−7326.
(98) Chen, M.; Zhang, D.; Hu, J.; Wang, H.; Zhang, Y.; Li, K.; Rong, Q.; Zhou, S.; Zhang, J.; Zhu, Z.; Liu, Q. Excellent Toluene Gas Sensing Properties of Molecular Imprinted Ag-$LaFeO_3$ Nanostructures Synthesized by Microwave-Assisted Process. *Mater. Res. Bull.* **2019**, *111*, 320−328.
(99) Chen, M.; Zhang, Y.; Zhang, J.; Li, K.; Lv, T.; Shen, K.; Zhu, Z.; Liu, Q. Facile Lotus-Leaf-Templated Synthesis and Enhanced Xylene Gas Sensing Properties of Ag-$LaFeO_3$ Nanoparticles. *J. Mater. Chem. C Mater.* **2018**, *6* (23), 6138−6145.
(100) Chen, M.; Zhang, Y.; Lv, T.; Li, K.; Zhu, Z.; Zhang, J.; Zhang, R.; Liu, Q. Ag-$LaFeO_3$ Nanoparticles Using Molecular Imprinting Technique for Selective Detection of Xylene. *Mater. Res. Bull.* **2018**, *107*, 271−279.
(101) Jaouali, I.; Hamrouni, H.; Moussa, N.; Nsib, M. F.; Centeno, M. A.; Bonavita, A.; Neri, G.; Leonardi, S. G. $LaFeO_3$ Ceramics as Selective Oxygen Sensors at Mild Temperature. *Ceram. Int.* **2018**, *44* (4), 4183−4189.
(102) Anajafi, Z.; Naseri, M.; Neri, G. Optical, Magnetic and Gas Sensing Properties of $LaFeO_3$ Nanoparticles Synthesized by Different Chemical Methods. *J. Electron. Mater.* **2019**, *48* (10), 6503−6511.
(103) Xiangfeng, C.; Siciliano, P. CH3SH-Sensing Characteristics of $LaFeO_3$ Thick-Film Prepared by Co-Precipitation Method. *Sens Actuators B Chem.* **2003**, *94* (2), 197−200.
(104) Alharbi, A. A.; Sackmann, A.; Weimar, U.; Bârsan, N. A Highly Selective Sensor to Acetylene and Ethylene Based on $LaFeO_3$. *Sens Actuators B Chem.* **2020**, *303*, 127204.

https://doi.org/10.1021/acsomega.4c00334
ACS Omega 2024, 9, 29994−30014